Journal of Organometallic Chemistry 1022 (2024) 123375

Contents lists available at ScienceDirect

Journal of Organometallic Chemistry

journal homepage: www.elsevier.com/locate/jorganchem

N—O bond cleavage and N_2 activation reactions of the Nitrosyl-Bridged complex $[Mo_2Cp_2(\mu\text{-}P^tBu_2)(\mu\text{-}NO)(NO)_2]$

M. Angeles Alvarez, M. Esther García, Daniel García-Vivó *, Ana M. Guerra, Miguel A. Ruiz *

Departamento de Química Orgánica e Inorgánica/IUQOEM, Universidad de Oviedo, E-33071 Oviedo, Spain

ARTICLE INFO

Keywords:
Nitrosyl complexes
Dinitrogen complexes
Carbonyl complexes
Nitroxyl complexes
Amide complexes
Phosphoraniminate complexes

ABSTRACT

The title compound was prepared through a three-step procedure starting with the hydride complex $[Mo_2Cp_2(\mu\text{-}H)(\mu\text{-}P^tBu_2)(CO)_4]$, which was first dehydrogenated through reaction with $HBF_4{\cdot}OEt_2$ to give the unsaturated complex $[Mo_2Cp_2(\mu\text{-}P^tBu_2)(CO)_4](BF_4)$ (Mo=Mo), which displays a transoid structure according to experimental (Mo-Mo = 2.8283(7) Å) and Density Functional Theory studies. The latter was then reacted with NO to give the dinitrosyl derivative $[Mo_2Cp_2(\mu\text{-}P^tBu_2)(CO)_2(NO)_2](BF_4)$, which in turn was further decarbonylated and nitrosylated upon reaction with $[N(PPh_3)_2]NO_2$ to give the title nitrosyl-bridged complex (Mo-Mo = 2.905(1) Å). This complex displayed a structure comparable to that of its PCy_2-bridged analogue, with similar pyramidalization of the bridging nitrosyl, but a more pronounced folding of the central MoPMoN skeleton and bending of terminal nitrosyls. It also displayed a similar N—O bond activation chemistry, as shown by its reactions with $HBF_4{\cdot}OEt_2$ to give the nitroxyl-bridged complex $[Mo_2Cp_2(\mu\text{-}P^tBu_2)(\mu\text{-}k^1{:}\eta^2\text{-}HNO)(NO)_2](BF_4)$ (HN—*O* = 1.330(8) Å), with $P(OEt)_3$ to give the phosphoraniminate-bridged complex $[Mo_2Cp_2(\mu\text{-}P^tBu_2)\{\mu\text{-}NP(OEt)_3\}(NO)_2]$, and with Na(Hg) to give the amide-bridged derivative $[Mo_2Cp_2(\mu\text{-}P^tBu_2)(\mu\text{-}NH_2)(NO)_2]$. Under a nitrogen atmosphere, however, the latter reaction also gave a minor side product identified as the dinitrogen-bridged derivative $[Mo_4Cp_4(\mu\text{-}P^tBu_2)_2(\mu_4\text{-}N_2)(NO)_4]$. This tetranuclear complex displays a dinitrogen molecule bridging four metal atoms in the novel $\mu_4\text{-}k^1{:}k^1{:}k^1{:}k^1$ coordination mode, with strong metal-nitrogen interactions taking the N_2 ligand to the diazendiide (N_2^{2-}) limit (N—*N* = 1.241(3) Å).

1. Introduction

Nitric oxide (NO) is an apparently simple molecule that can bind one or several metal atoms in many different ways, so its coordination chemistry itself is of great academic interest [1]. This gas, however, also is a side product formed in many large-scale activities and processes with undesirable effects on health and environment, which makes it an important air pollutant requiring catalytic abatement [2]. The latter rely typically on heterogeneous interactions of the gas with one or several atoms of metal surfaces. In this context, the study at the molecular level of nitrosyl complexes with unusual geometries that can undergo N—O bond cleavage reactions under mild conditions is a matter of interest in the search for new strategies to build more efficient catalysts for NO abatement. In particular, the study of transformations of nitric oxide at binuclear complexes possibly provides the simplest models for the interaction of this molecule with the surface of heterogeneous metal catalysts [3].

We have previously reported the synthesis and reactivity of the PCy_2-bridged binuclear trinitrosyl complexes $[M_2Cp_2(\mu\text{-}PCy_2)(\mu\text{-}NO)(NO)_2]$ (Mo, W). These molecules can be made in a two-step procedure starting from the corresponding hydride complexes $[M_2Cp_2(\mu\text{-}H)(\mu\text{-}PCy_2)(CO)_4]$ (Scheme 1), and display a bridging nitrosyl with an unusual pyramidalization at the N atom, thought to be related with several and relatively uncommon N—O bond cleavage processes, such as those observed upon reaction with different reductants, CO, and phosphites, whereby the nitrosyl ligand is transformed into amide (NH_2), and phosphoraniminate ($NP(OR)_3$) ligands [4]. On the other hand, we have also found recently that the bulky P^tBu_2 ligand can stabilize binuclear nitrosyl complexes undergoing unusual N—O bond cleavage processes [5,6], not observed when using analogous complexes having bridging PCy_2 ligands. It was thus of interest to see the effect that replacement of the PCy_2 ligand in the above trinitrosyl complexes with the bulkier P^tBu_2 one would have on the structure (particularly on the pyramidalization at the bridging nitrosyl) and N—O bond activation reactions of the complex, which is the purpose of the present paper. As it will be shown below, the presence of P^tBu_2 ligands in these trinitrosyl complexes has significant structural

* Corresponding author at: Departamento de Química Orgánica e Inorgánica/IUQOEM, Universidad de Oviedo, E-33071 Oviedo, Spain.
E-mail addresses: garciavdaniel@uniovi.es (D. García-Vivó), mara@uniovi.es (M.A. Ruiz).

https://doi.org/10.1016/j.jorganchem.2024.123375
Received 22 July 2024; Received in revised form 5 September 2024; Accepted 6 September 2024
Available online 17 September 2024

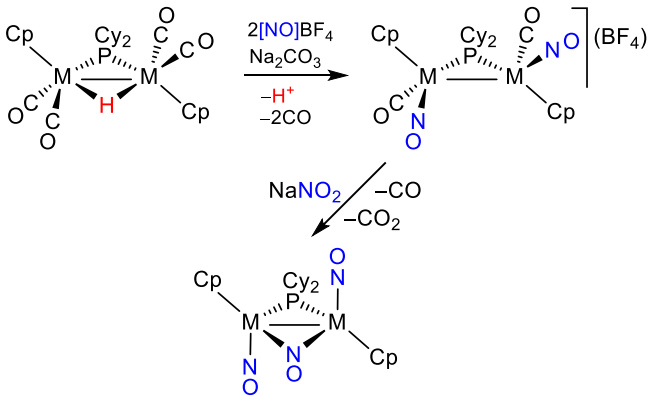

Scheme 1. Formation of PCy_2-bridged trinitrosyl complexes (M = Mo, W).

effects, but not on the bridging nitrosyl. As a result, the reactivity is not modified substantially either, except for the occurrence of an interesting side-reaction that involves denitrosylation and dinitrogen coordination to give a tetranuclear complex providing a new coordination mode of the dinitrogen molecule.

2. Results and discussion

2.1. Synthesis and structural characterization of cationic precursors $[Mo_2Cp_2(\mu\text{-}P^tBu_2)(CO)_4]^+$ (2) and $[Mo_2Cp_2(\mu\text{-}P^tBu_2)(CO)_2(NO)_2]^+$ (3)

To prepare the cationic dinitrosyl precursor of the targeted trinitrosyl complex, we have followed the method recently implemented by us to obtain related ditungsten species [5]. This starts in our case with the known hydride complex $[Mo_2Cp_2(\mu\text{-}H)(\mu\text{-}P^tBu_2)(CO)_4]$ (**1**) [7,8], which is first dehydrogenated upon reaction with $HBF_4{\cdot}OEt_2$ to give the unsaturated cationic complex $[Mo_2Cp_2(\mu\text{-}P^tBu_2)(CO)_4](BF_4)$ (**2-BF$_4$**). In a second step, the latter compound is reacted with nitrogen monoxide (5 % in N_2) to yield the desired dinitrosyl precursor $[Mo_2Cp_2(\mu\text{-}P^tBu_2)(CO)_2(NO)_2](BF_4)$ (**3-BF$_4$**) in good yield (Scheme 2). These BF_4^- salts can be used without further purification. Moreover, they can be converted into the corresponding BAr'_4^- salts **2-BAr'$_4$** and **3-BAr'$_4$** through anion exchange with $NaBAr'_4$ in dichloromethane solution (Ar' = 3, 5-$C_6H_3(CF_3)_2$). This enables their easier crystallization or chromatographic purification, hence the isolation of very pure samples of these cationic complexes. We note that the cation **3** is present in solution as a dominant symmetrical isomer (see below), in contrast to its PCy_2-bridged analogue, for which a second, asymmetrical isomer co-exists in solution in significant amounts [4]. We attribute this difference to the higher steric demands of the P^tBu_2 ligand, compared to the PCy_2 one.

The unsaturated cation **2** belongs to a family of complexes of general

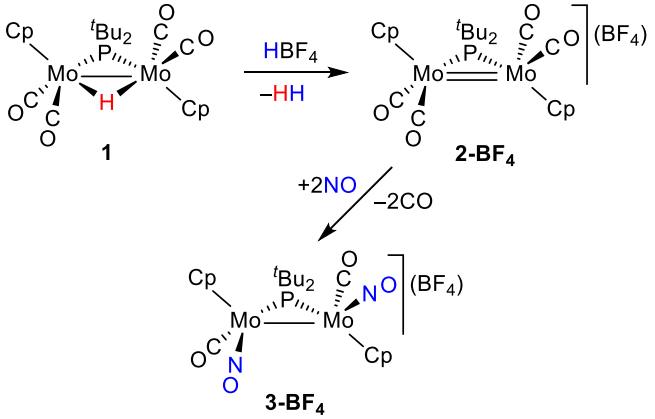

Scheme 2. Preparation of cationic intermediates **2-BF$_4$** and **3-BF$_4$**.

formula $[M_2Cp_2(\mu\text{-}PRR')(CO)_4]^+$ (M = Mo, W; RR' = Ph_2, Cy_2, MesH, CyH) prepared previously by us [9]. These 32 electron complexes can be formed through either oxidation or protonation of the corresponding hydride precursors $[M_2Cp_2(\mu\text{-}H)(\mu\text{-}PRR')(CO)_4]$ and could not be structurally characterized at the time, as they are products of reduced stability (also depending on R and M). A cisoid arrangement of the $MCp(CO)_2$ fragments in these cations was proposed on the basis of NMR data. Fortunately, the higher bulkiness and electron-releasing properties of the ^{t}Bu groups in **2-BAr'$_4$** makes this complex stable enough to render X-ray-quality crystals, therefore enabling full determination of its molecular structure, which turned to be different than anticipated, as the $MoCp(CO)_2$ fragments of the cation are found in a rather transoid arrangement.

The structure of the cation in the crystal of **2-BAr'$_4$** (Fig. 1 and Table 1) is built from two $MoCp(CO)_2$ fragments bridged by a P^tBu_2 ligand in an essentially symmetric way (Mo–P ca. 2.47 Å). All of this configures a 32 electron complex for which a metal-metal double bond has to be proposed according to the 18 electron rule, which is consistent with the short intermetallic separation of 2.8283(7) Å, some 0.4 Å shorter than the corresponding distance in its electron-precise precursor **1** (3.247(1) Å) [7], or that in the unbridged dimer $[Mo_2Cp_2(CO)_4]$ (3.235(1) Å) [10]. This distance, however, falls in the upper part of the range of 2.55–2.80 Å most commonly found for Mo_2 or W_2 organometallic complexes formally bearing double bonds [11], an effect possibly due to the large steric pressure introduced in the molecule by the bulky P^tBu_2 ligand. The relative arrangement of the $MoCp(CO)_2$ fragments, if taking the Mo_2P plane as the reference, is of a transoid type, as noted above, but both fragments are clearly inequivalent. The C1 and C4 carbonyl atoms occupy almost antiparallel positions, with similar P-M-C and M-M-C angles of ca. 100 and 80° respectively. In contrast, the C3 atom on Mo2 points away from the intermetallic region (Mo1-Mo2-C3 = 123.3(2)°), whereas the C2 atom on Mo1 adopts an incipient bent semibridging interaction with the Mo2 atom (C2···Mo2 = 2.842(7) Å; Mo1-C2-O2 = 170.2(6)°), as indicated by the acute Mo2-Mo1-C2 angle of 69.8(2)°, below the limiting value of 75° characterizing such a type of interaction [12]. As a result of it, the C2 atom occupies a transoid position relative to the P atom (P-Mo1-C2 = 123.1(2)°), whereas the C3 atom is positioned *cis* to it (P-Mo2-C3 = 70.9(2)°). At the same time, the Cp ligand bound to Mo1 adopts a position almost centred on the intermetallic axis, very different from the one exhibited by the second Cp ring.

The IR spectra for compounds **2-BF$_4$** and **2-BAr'$_4$** (Table 2) display

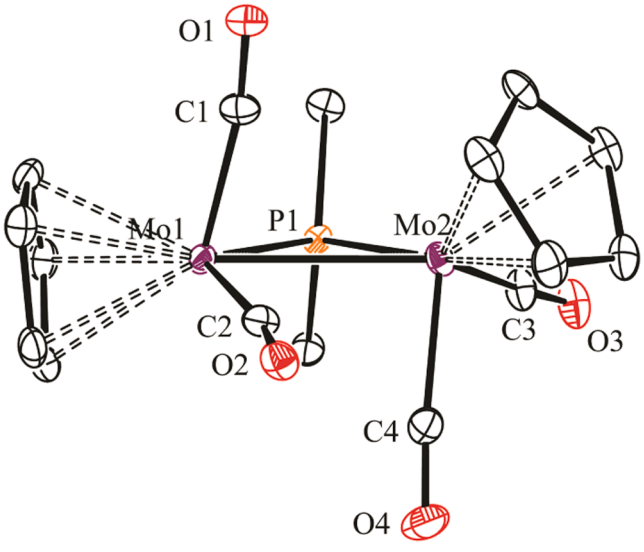

Fig. 1. ORTEP diagram (30 % probability) of the cation in compound **2-BAr'$_4$**, with ^{t}Bu groups (except their C^1 atoms) and H atoms omitted for clarity.

Table 1
Selected bond lengths (Å) and angles (°) for compound **2-BAr'$_4$**.

Mo1-Mo2	2.8283(7)	Mo1-P1-Mo2	69.83(4)
Mo1-P1	2.468(2)	P1-Mo1-C1	97.4(2)
Mo2-P1	2.474(2)	P1-Mo1-C2	123.1(2)
Mo1-C1	1.984(7)	P1-Mo2-C3	70.9(2)
Mo1-C2	1.997(7)	P1-Mo2-C4	100.6(2)
Mo2-C3	1.982(7)	Mo2-Mo1-C1	76.9(2)
Mo2-C4	1.996(7)	Mo2-Mo1-C2	69.8(2)
Mo2···C2	2.842(7)	Mo1-Mo2-C3	123.3(2)
		Mo1-Mo2-C4	84.4(2)
		Mo1-C2-O2	170.2(6)

Table 2
Selected IR and $^{31}P\{^1H\}$ NMR data for new compounds.[a].

Compound	ν(XO)	δ (P)
$[Mo_2Cp_2(\mu\text{-}P^tBu_2)(CO)_4](BF_4)$ (**2-BF$_4$**)	2006 (m), 1955 (vs), 1937 (s, sh), 1913 (m, sh)	233.5
$[Mo_2Cp_2(\mu\text{-}P^tBu_2)(CO)_4](BAr'_4)$ (**2-BAr'$_4$**)	2006 (m), 1952 (vs), 1941 (s), 1908 (w)	233.7
$[Mo_2Cp_2(\mu\text{-}P^tBu_2)(CO)_2(NO)_2](BF_4)$ (**3-BF$_4$**)	2027 (vs), 1964 (w, br), 1677 (vs)	319.6
$[Mo_2Cp_2(\mu\text{-}P^tBu_2)(CO)_2(NO)_2](BAr'_4)$ (**3-BAr'$_4$**)	2029 (s), 1700 (m, sh), 1680 (vs)	322.6
$[Mo_2Cp_2(\mu\text{-}P^tBu_2)(\mu\text{-NO})(NO)_2]$ (**4**)	1618 (w, sh), 1589 (vs)[b]	255.7
cis-$[Mo_2Cp_2(\mu\text{-}P^tBu_2)(\mu\text{-NO})(NO)_2]$ (***cis*-4**)	1639 (vs), 1570 (m, sh)	262.2
$[Mo_2Cp_2(\mu\text{-}P^tBu_2)(\mu\text{-}k^1;\eta^2\text{-HNO})(NO)_2]$ (**5-BF$_4$**)	1682 (m, sh), 1658 (vs)	302.9
$[Mo_2Cp_2(\mu\text{-}P^tBu_2)(\mu\text{-}k^1;\eta^2\text{-HNO})(NO)_2]$ (**5′-BF$_4$**)[c]		294.1
$[Mo_2Cp_2(\mu\text{-}P^tBu_2)\{\mu\text{-NP(OEt)}_3\}(NO)_2]$ (**6**)	1553 (m, sh), 1527 (vs)	264.7 (s), 25.3 (s)
$[Mo_2Cp_2(\mu\text{-}P^tBu_2)(\mu\text{-NH}_2)(NO)_2]$ (**7**)	1574 (m, sh), 1547 (vs)	256.8
$[Mo_4Cp_4(\mu\text{-}P^tBu_2)_2(\mu\text{-}k^1;k^1;k^1\text{-}N_2)(NO)_4]$ (**8**)	1556 (vs)	266.1

[a] IR spectra recorded in dichloromethane solution, unless otherwise stated, with stretching frequencies of NO and CO ligands (ν(XO), X = C, N) given in wave numbers (cm^{-1}); NMR spectra recorded in CD_2Cl_2 solution at 121.48 MHz and 295 K, unless otherwise stated, with chemical shifts (δ) in ppm relative to external 85 % aqueous H_3PO_4.

[b] The bridging nitrosyl ligand gives rise to a N—O stretch at 1407 cm^{-1} in KBr disk.

[c] Minor isomer formed along with **5-BF$_4$** (see text).

four C—O stretches which are similar to each other, indicating little anion-cation interactions in solution, and are consistent with the structure found in the crystal. In particular, the medium intensity of the highest-frequency band of these complexes (at 2006 cm^{-1}) is indicative of a transoid arrangement of the $M(CO)_2$ oscillators of the molecule [13]. Moreover, the appearance of a relatively low-frequency band at ca. 1910 cm^{-1} is consistent with the presence of a weak semibridging interaction for one of the carbonyl ligands, as found in the crystal. In agreement with all of this, the gas-phase optimized structure of the cation **2** using Density Functional Theory (DFT) methods (see the experimental section) is in good agreement with the structure found in the crystal (Fig. 2), as they are the relative intensities and frequencies of the computed C—O stretches (Figure S7). A pure transoid structure with equivalent $MoCp(CO)_2$ fragments (approximate C_2 symmetry, as depicted in Scheme 2) proved to be not a minimum in the potential energy surface of the system, likely due to unfavourable repulsive interactions of CO and Cp ligands with the bulky ^{t}Bu groups. On the other hand, our calculations indicate that a cisoid structure would display also a semibridging carbonyl, while its Gibbs free energy would be some 10 kJ/mol higher than the transoid one (Fig. 2). Moreover, the computed C—O stretches for the latter structure indicate that the highest-frequency stretch should also be the strongest one (Figure S7), as expected for a cisoid arrangement of the $M(CO)_2$ oscillators of the molecule [13], this being inconsistent with the experimental spectra of the salts of **2** in solution. Since all experimental spectra previously reported for cations of type $[M_2Cp_2(\mu\text{-PRR})(CO)_4]^+$ display C—O stretching patterns comparable to that of **2** (particularly as concerning the medium-intensity of its highest-frequency C—O stretch), we must conclude that all these cations also display an essentially transoid structure in solution, and not the cisoid one proposed at the time [9].

The NMR data for the cation **2**, however, indicates dynamic behaviour in solution, as the Cp and ^{t}Bu groups appear as equivalent in the room temperature NMR spectra, while the four inequivalent CO ligands just give rise to a very broad ^{13}C resonance at 229.5 ppm (see the Experimental Section). On lowering the temperature, the Cp and ^{t}Bu resonances in the ^{1}H NMR spectrum of **2-BAr'$_4$** broaden progressively, and eventually split into two sets of the same intensity, in agreement with the static structure of the cation. In addition, the ^{13}C NMR spectrum of the complex recorded at 203 K displays, apart from separated Cp and ^{t}Bu resonances, separate resonances for each of the four inequivalent carbonyls of the molecule, at 242.7 (s), 228.4 (d, J_{CP} = 44), 227.1 (d, J_{CP} = 6) and 221.2 (s) ppm (Figure S14). The most deshielded resonance can be safely assigned to the semibridging carbonyl, and its negligible P-C coupling is consistent with its transoid positioning relative to the P atom (P-Mo1-C2 = 123.1(2)^o in the crystal). Besides this, the strong coupling of the 228.4 ppm resonance allows its assignment to the unique carbonyl

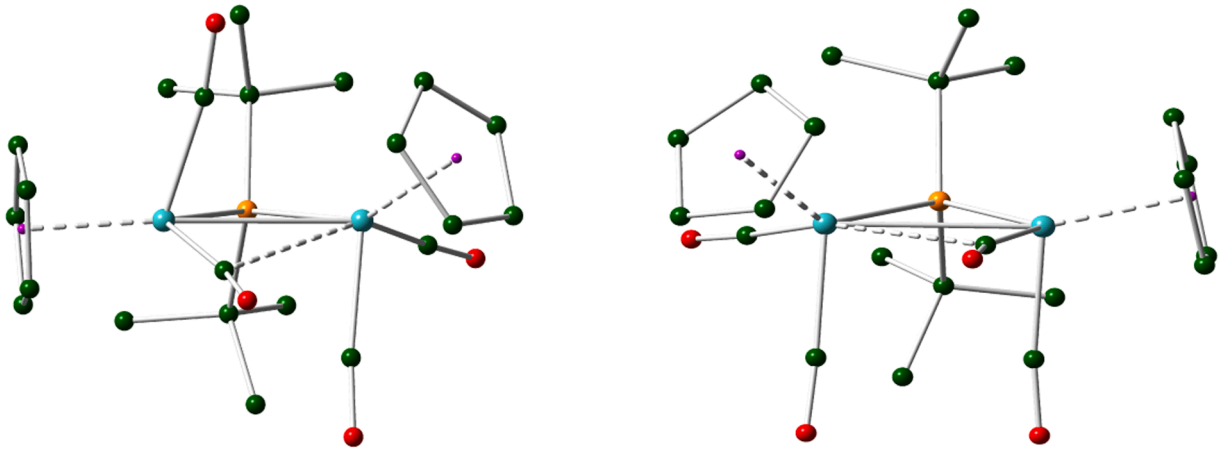

Fig. 2. M06L-DFT computed structure of the cation **2** (left), and its cisoid isomer (right), with H atoms omitted for clarity. Colour code: Mo(turquoise), P(orange), C (green), O(red). Relative Gibbs free energies were 0 and +9 kJ/mol in the gas phase at 298 K.

displaying an acute (cisoid arrangement) angle relative to the P atom (P-Mo2-C3 = 70.9(2)° in the crystal) [14,15]. From the corresponding coalescence data for the Cp resonances in the ^{1}H spectrum (T_c = 230 K, $\Delta\nu$ = 69 Hz), a quite low activation barrier of 46 ± 0.5 kJ/mol can be estimated for the corresponding dynamic process [16]. For the latter we propose a concerted rotation of the $MoCp(CO)_2$ fragments averaging the pairs of Cp and ^{t}Bu resonances, which also implies a pairwise averaging of carbonyl resonances (Scheme 3). The observation of an unique broad carbonyl resonance in the room temperature spectrum of **2-BAr'$_4$** indicates the occurrence of an additional, slower dynamic process involving full exchange of all four carbonyl sites, not further investigated.

Spectroscopic data for compounds **3-BF$_4$** and **3-BAr'$_4$** (Table 2 and Experimental Section) are again comparable to each other and moreover indicative of the presence of a very major symmetrical isomer in solution having equivalent Cp, ^{t}Bu and CO pairs, then deserving no specific comments. We just note that the structure of this type of isomer was determined by X-ray diffraction on the PPh_2-bridged analogue $[Mo_2Cp_2(\mu\text{-}PPh_2)(CO)_2(NO)_2](BF_4)$ [17]. In the case of the cation **3**, the positioning of the equivalent carbonyls *cis* to the P atom is indicated by the observation of a relatively large two-bond P-C coupling of 21 Hz in its unique CO resonance at 220.1 ppm [14,15].

2.2. Synthesis and structural characterization of the trinitrosyl complex $[Mo_2Cp_2(\mu\text{-}P^tBu_2)(\mu\text{-}NO)(NO)_2]$ (4) and its cis isomer

Compound **4** was prepared as previously implemented for its PCy_2-bridged analogue, that is, through the nucleophilic attack of the nitrite anion on the cationic dicarbonyl complex **3-BF$_4$** in dichloromethane solution (Scheme 4). However, instead of $NaNO_2$, a CH_2Cl_2-soluble nitrite salt as $PPN(NO_2)$ (PPN = $N(PPh_3)_2$) had to be used for a fast reaction in this case. In that way, the trinitrosyl complex **4** can be obtained as a dark blue solid in 75 % yield after chromatographic workup. Attempts to obtain a related ditungsten complex were unsuccessful: although the reaction of the known complex $[W_2Cp_2(\mu\text{-}P^tBu_2)(CO)_2(NO)_2](BF_4)$ [5] with $PPN(NO_2)$ at room temperature gave first a bluish solution, this rapidly turned yellow, indicating that the targeted trinitrosyl complex was indeed formed, but it was rather unstable under these experimental conditions. No further attempts to isolate this product were made.

Irradiation of **4** with visible-UV light in toluene solution caused its rearrangement into its *cis*-dinitrosyl isomer ***cis*-4**. Unlike its PCy_2-bridged analogue [4], full isomerization could not be achieved in this case, as a photochemical equilibrium is reached, with the maximum ***cis*-4**/**4** ratio being ca. 2/1. Unfortunately, isomer ***cis*-4** could not be fully separated from its transoid isomer through chromatography; in fact, it reverts to **4** progressively upon chromatographic workup even at 253 K. Therefore, only partial spectroscopic data were obtained for this more energetic isomer. As expected, heating toluene solutions of ***cis*-4** promoted its full rearrangement back into the more stable isomer **4** (full conversion in ca. 2 h at 353 K).

The structure of **4** in the crystal (Fig. 3 and Table 3) is very similar to that of its PCy_2-bridged analogue, and deserves no detailed comments, except for some changes derived from the replacement of Cy groups with the bulkier and better electron-releasing ^{t}Bu groups at the bridging P atom. Firstly, we note that Mo-P distances in **4** are ca. 0.05 Å longer, which is an expected steric effect of the ^{t}Bu groups. Secondly, it can be

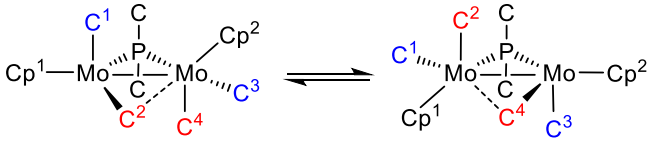

Scheme 3. Schematic representation of the fast fluxional process proposed for the cation **2**, emphasizing the pairwise exchange of Cp and CO ligands.

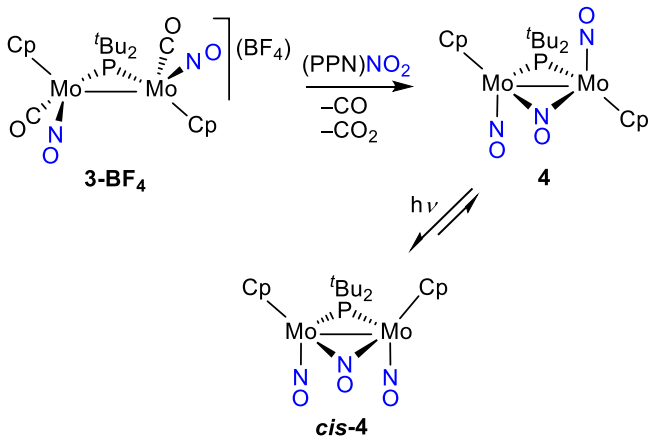

Scheme 4. Formation of complexes **4** and ***cis*-4**.

appreciated that the central skeleton in **4** is significantly more folded (β = 152.5° vs. 164.4°), with concomitant stronger department of the terminal nitrosyls from their antiparallel arrangement (Mo-Mo-N angles of ca. 84 and 110°). This is again an structural effect derived from the presence of bridging ligands with high steric demands, previously found in different dicarbonyl complexes of type $[M_2Cp_2(\mu\text{-}X)(\mu\text{-}PR_2)(CO)_2]$ [18]. Finally, we note that the increased electron density introduced by the P^tBu_2 ligand (vs. PCy_2), has no significant effect on the pyramidalization degree of the bridging nitrosyl ligand, which is similar to the one measured in the PCy_2-bridged complex (0.21 vs. 0.22). Instead, this increased electron density seems to have a more pronounced effect on the terminal nitrosyls, which display a moderate but significantly higher bending (M-N-O angles of ca. 168° vs. 175°). Thus, a similar μ-NO-based reactivity can be anticipated for this complex.

Spectroscopic data for compound **4** in solution (Table 2 and Experimental section) are comparable to those of its PCy_2-bridged analogue, except for the changes anticipated from the replacement of the PCy_2 ligand with the P^tBu_2 one (decrease in N—O stretches and increase in the ^{31}P chemical shift), and deserves no detailed comments. We just note that the NMR data for **4** indicate the equivalence of Cp and ^{t}Bu groups in the molecule, this requiring the operation of a fast dynamic process that inverts the folding of its central MoPMo(μ-N) skeleton. This would render an effective C_2 symmetry axis passing through the bridgehead P and N atoms, as proposed previously for several dicarbonyl complexes of type $[M_2Cp_2(\mu\text{-}X)(\mu\text{-}PR_2)(CO)_2]$ having similarly folded central skeletons [18].

As for isomer ***cis*-4**, we note that the cisoid disposition of the terminal nitrosyls can be deduced from the relative intensities of the N—O stretches present in its IR spectrum (strong and medium, in order of decreasing frequencies) [13,19], while its ^{1}H NMR spectrum displays equivalent Cp ligands but inequivalent ^{t}Bu groups, as expected. The resonance of one of these groups (at 1.16 ppm) is broad, which denotes hindered rotation of one of the ^{t}Bu groups (likely the one closer to both Cp ligands) around the P-CMe_3 bond, an effect previously observed also for the structurally related chloride-bridged complex *cis*-$[Mo_2Cp_2(\mu\text{-}Cl)(\mu\text{-}P^tBu_2)(NO)_2]$ [20].

Both **4** and ***cis*-4** are deep-blue coloured compounds, as previously found for their PCy_2-bridged analogues. In the latter case, this unexpected feature was related at the time to the relatively low HOMO-LUMO separation of some 2.9 eV, as computed by DFT methods [4a]. We have now performed TD-DFT calculations on **4** to gain further insight into this matter, to find that the colour of the complex is indeed related to an even lower HOMO-LUMO gap of the molecule. More precisely, the molecule is computed to give rise to a broad absorption in the visible region centred at ca. 550 nm (expt. broad absorption centred at ca. 600 nm in CH_2Cl_2 solution). This would result from transits to the LUMO (with large π^*(N—O) character of the bridging nitrosyl) from

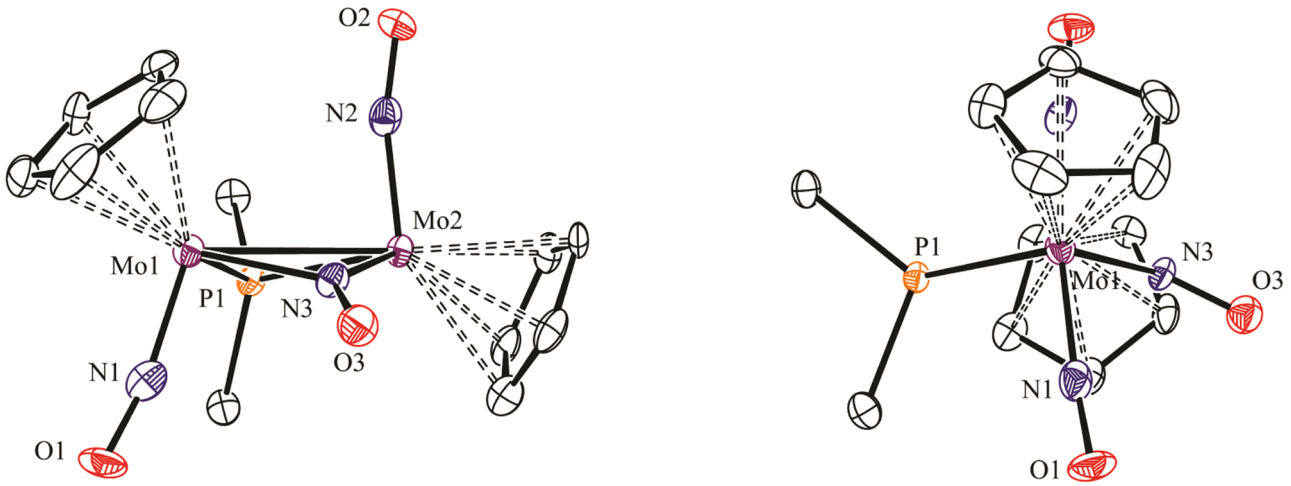

Fig. 3. ORTEP diagram (30 % probability) of compound **4**, with ^{t}Bu groups (except their C^{1} atoms) and H atoms omitted for clarity. On the right, a view of the molecule from the Mo1-Mo2 vector.

Table 3
Selected bond lengths (Å) and angles (°) for compound **4** and its PCy_2-bridged analogue **4-Cy**.

parameter	4	4-Cy[a]
Mo1-Mo2	2.905(1)	2.8935(3)
Mo1-P1	2.467(4)	2.4063(7)
Mo2-P1	2.463(3)	2.4155(7)
Mo1-N3	2.05(1)	2.031(2)
Mo2-N3	1.99(1)	2.018(2)
Mo1-N1	1.78(2)	1.784(2)
Mo2-N2	1.79(1)	1.798(2)
N3-O3	1.23(2)	1.227(3)
Mo1-Mo2-N2	83.6(4)	88.9(1)
Mo2-N2-O2	166(1)	176.1(2)
Mo2-Mo1-N1	110.3(4)	105.4(1)
Mo1-N1-O1	169(1)	173.3(2)
∑(N3)[b]	358.0	357.5
α(*pd*)[c]	168.4(0.21)	167.8 (0.22)
β[d]	152.5	164.4

[a] Data for **4-Cy** taken from reference 4a.
[b] Summation of bond angles around N3.
[c] Angle (α) defined by the bridging NO ligand and the centroid (ct) of the Mo-Mo bond; the pyramidalization degree (pd) of the bridging NO ligand is defined as (180-α)/54.75 (see reference 4a).
[d] Folding angle of the central MoPMoN3 skeleton, defined by the P1-ct-N3 or P-Mo-Mo-N3 angles.

frontier MOs close to the HOMO (mainly HOMO-1 to HOMO-3, with π(Mo-NO) character of the terminal nitrosyls, as well as σ(Mo-X) character; *X* = Mo, μ-N; see the Supplementary Material). The nature of the LUMO, in turn, suggests that population of this orbital (through reduction or addition of bases) should weaken preferentially the N—O bond of the bridging nitrosyl ligand, in agreement with some of the chemical reactions of **4** discussed below.

2.3. Protonation of compound 4

Compound **4** reacts with $HBF_4{\cdot}OEt_2$ in dichloromethane solution at room temperature or below to give the nitroxyl complex [Mo_2Cp_2(μ-P^{t}Bu$_2$)(μ-k^1:η^2-HNO)(NO)$_2$] (**5-BF$_4$**) (Scheme 5), which displays an unusual k^1:η^2-bridging coordination of the nitroxyl (HNO) ligand, as observed for its PCy_2-bridged analogue [4]. In this case, however, a second isomer **5′-BF$_4$**, with spectroscopic parameters analogous to those of the main product, coexists in solution, with the **5**/**5′** equilibrium ratio in CD_2Cl_2 being ca 5:1. Yet, pure samples of the main isomer could be obtained through crystallization. Attempts to obtain related

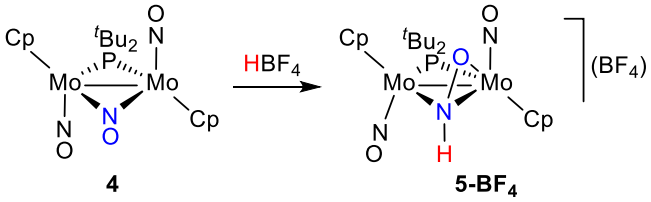

Scheme 5. Protonation reaction of compound **4**, only showing the major product (see text).

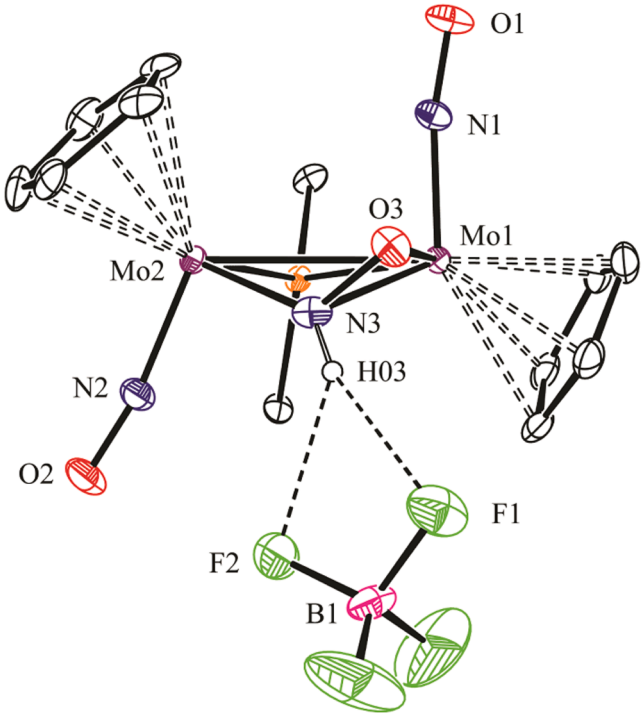

Fig. 4. ORTEP diagram (30 % probability) of the cation and anion of **5-BF$_4$** in the crystal lattice, with ^{t}Bu groups (except their C^{1} atoms) and most H atoms omitted for clarity, and N—H···F hydrogen bonding interactions indicated.

Table 4
Selected bond lengths (Å) and angles (°) for compound **5-BF$_4$**.

Mo1-Mo2	3.0213(7)	Mo1-P1-Mo2	73.73(4)
Mo1-P1	2.565(2)	Mo1-N3-Mo2	91.8(2)
Mo2-P1	2.470(2)	P1-Mo1-N1	92.2(2)
Mo1-N3	2.204(6)	P1-Mo1-N3	88.4(2)
Mo2-N3	1.998(6)	P1-Mo1-O3	120.1(2)
Mo1-N1	1.788(5)	P1-Mo2-N2	95.4(2)
Mo1-O3	2.086(5)	P1-Mo2-N3	96.0(2)
Mo2-N2	1.788(6)	N1-Mo1-N3	107.3(2)
N1-O1	1.197(7)	N2-Mo2-N3	90.1(3)
N2-O2	1.188(8)	Mo1-Mo2-N2	112.4(2)
N3-O3	1.330(8)	Mo2-N2-O2	169.8(6)
N3-H03	0.83(12)	Mo2-Mo1-N1	88.6(2)
F1···H03	2.34(13)	Mo1-N1-O1	168.3(6)
F2···H03	2.27(13)		

nitrosomethane-bridged complexes by reacting **4** with methylating reagents such as CF_3SO_3Me or $[Me_3O](BF_4)$ were unsuccessful, and only led to the protonation of the parent substrate.

The structure of the major isomer **5-BF$_4$** in the crystal (Fig. 4 and Table 4) is similar to that of its PCy_2-bridged analogue [4], which remains as the only other nitroxyl-bridged complex crystallographically characterized so far. As a result of the η^2 coordination of the ligand to a second Mo atom (Mo1-N3 = 2.204(6); Mo1-O3 = 2.086(5) Å), the N—O bond is enlarged (therefore weakened) to 1.330(8) Å, a figure similar to the one observed for its PCy_2-bridged analogue (1.348(6) Å), and substantially higher than the N—O distances of ca. 1.19–1.24 Å measured in the few mononuclear complexes with N-bound nitroxyl ligands characterized so far [21]. The latter in turn are comparable to the distance of 1.212 Å measured in free HNO, which is the reference length for a $N=O$ double bond [22]. In the crystal lattice, the N-bound H atom is involved in a bifurcated hydrogen bonding interaction with two F atoms of the BF_4^- counterion, with H···F distances of ca. 2.3 Å, expectedly longer than those observed in the more common (linear) N—H···F interactions (ca. 1.9 Å) [23].

Spectroscopic data in solution for compound **5-BF$_4$** (Table 2 and Experimental section) are consistent with the structure found in the solid state, and are also similar to those of its PCy_2-bridged analogue, therefore deserving only a few comments. Notably, its IR spectrum displays N—O stretches for the remaining terminal ligands some 70 cm^{-1} more energetic than those of its neutral precursor, as expected for a cationic species, while retaining the relative intensities of a transoid $[M(NO)]_2$ oscillator. The presence of the N-bound H atom is denoted by the appearance of a strongly deshielded and broad resonance at 12.20 ppm in its ^{1}H NMR spectrum, which otherwise indicates the absence of any symmetry elements in the molecule (inequivalence of Cp and ^{t}Bu pairs), as expected. The ^{1}H NMR spectrum of the minor isomer **5′-BF$_4$** also displays separated resonances for the Cp and ^{t}Bu groups, and the resonance corresponding to the added proton appears at 13.15 ppm, a chemical shift very close to that of the major isomer. Thus, we trust that this minor isomer also bears a k^1:η^2-bridging nitroxyl ligand. DFT calculations indicate that a structure similar to that of the cation **5**, but with the η^2-interaction shifted to the other molybdenum atom, has a Gibbs free energy only 4 kJ/mol higher than that of **5** (Fig. 5), and therefore seems the most likely structure for the cation in the minor isomer **5′-BF$_4$**. We note that this sort of isomerism was also proposed previously for the nitrosomethane-bridged complex $[Mo_2Cp_2(\mu\text{-}PCy_2)(\mu\text{-}k^1{:}\eta^2\text{-}MeNO)(NO)_2]^+$, although no DFT calculations were performed at the time [4].

2.4. Reaction of complex 4 with P(OEt)$_3$

The PCy_2-bridged analogue of **4** proved to be unreactive towards phosphines, but reacted with phosphites to render rare bridging phosphoraniminate ligands, after cleavage of the N—O bond of the bridging nitrosyl and formation of new N-P bonds [4]. We have found that **4** behaves similarly, but only the reaction with $P(OEt)_3$ was studied in detail. The latter takes place slowly in refluxing toluene solution and using a large excess of reagent to give the corresponding phosphoraniminate-bridged complex $[Mo_2Cp_2(\mu\text{-}P^tBu_2)\{\mu\text{-}NP(OEt)_3\}(NO)_2]$ (**6**) as major organometallic product (Scheme 6), along with trielthyl phosphate, as determined by inspection of the crude reaction mixture by ^{31}P NMR spectroscopy. Compound **6** proved to be a stable product that could be isolated as a pure yellow solid after chromatographic workup in ca. 40 % yield. Spectroscopic data for this product (Table 2 and experimental section) are comparable to those of their PCy_2-bridged analogues $[Mo_2Cp_2(\mu\text{-}PCy_2)\{\mu\text{-}NP(OR)_3\}(NO)_2]$ (R = Et, Ph), the structure of which was determined by X-ray diffraction analysis on the triphenyl phosphite derivative [4]. The salient spectroscopic feature for **6** is the presence in the ^{31}P spectrum of a relatively shielded resonance at 25.3 ppm corresponding to the phophoraniminate ligand,

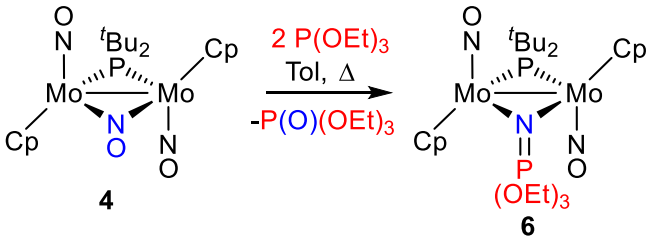

Scheme 6. Reaction of compound **4** with $P(OEt)_3$.

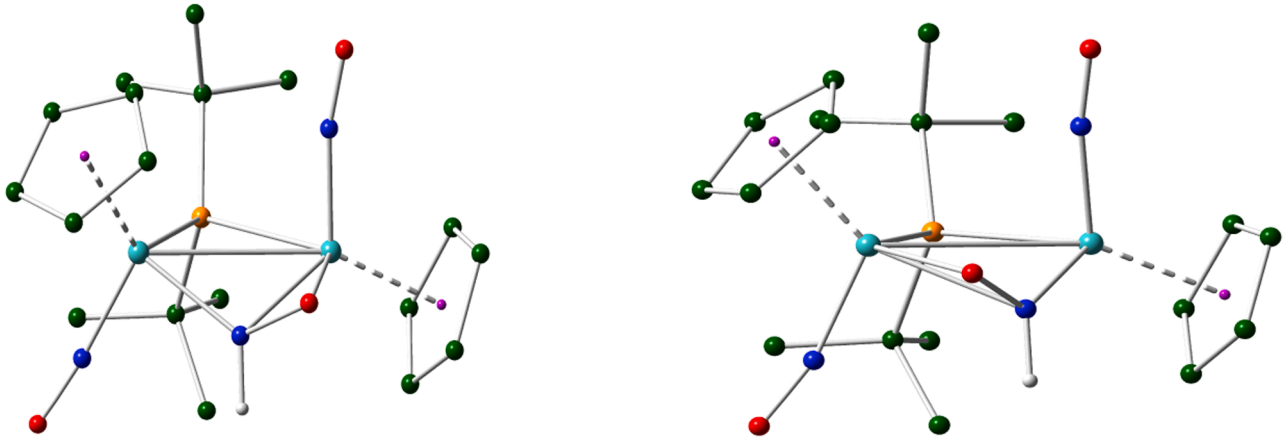

Fig. 5. M06L-DFT computed structures of the cation 5 (left) and its isomer 5′ (right), with most H atoms omitted for clarity. Colour code: Mo(turquoise), P(orange), C (green), N(blue), O(red), H(white). Relative Gibbs free energies were 0 and +4 kJ/mol in the gas phase at 298 K.

in addition to the strongly deshielded P^{t}Bu$_2$ resonance at 264.7 ppm. The methylenic protons of the iminate ligand are inequivalent, as expected for the transoid geometry of the complex (lacking a plane of symmetry), the latter being also indicated by the relative intensities observed in the IR spectrum for the N—O stretches of the remaining nitrosyl ligands.

2.5. Reduction reactions of compound 4

The PCy$_2$-bridged analogue of **4** has been shown previously to be reduced with either Na(Hg) or Zn(Hg) amalgams (0.5 % by weight) in tetrahydrofuran (THF) solutions to yield the amide-bridged derivative [Mo$_2$Cp$_2$(μ-PCy$_2$)(μ-NH$_2$)(NO)$_2$] as the unique product, with the isolated yield being improved by adding a little water to the solvent [4]. Compound **4** behaved analogously when reacting with Na(Hg) to give the corresponding amide-bridged derivative [Mo$_2$Cp$_2$(μ-P^{t}Bu$_2$)(μ-NH$_2$)(NO)$_2$] (**7**) as the very major product (Scheme 7). However, it reacted very slowly with the milder reductant zinc amalgam (also to give **7**), a difference that can be understood by considering that the better electron-releasing properties of the P^{t}Bu$_2$ ligand (when compared to the PCy$_2$ one) should make the reduction of **4** a somewhat more difficult process. Still more interesting, we noticed that in the reduction of **4** with Na amalgam under the usual argon atmosphere a very minor product was usually formed along with **7** (typically in a ratio of ca. 1:20 relative to **7**). This minor product could be separated chromatographically thanks to its deep purple colour, and it has been characterized as the dinitrogen-bridged complex [Mo$_4$Cp$_4$(μ-P^{t}Bu$_2$)$_2$(μ-k^1:k^1:k^1:k^1-N$_2$)(NO)$_4$] (**8**), which exhibits a novel coordination mode for the N$_2$ ligand (see below).

Separated experiments indicated the following: (a) Compound **8** does not further react with Na amalgam, therefore it is not an intermediate in the formation of **7**. (b) The relative amount of **8** in the final reaction mixture goes to zero when using pure toluene as reaction solvent. (c) The relative amount of **8** in the final reaction mixture increases (to ca. 1:5 relative to **7**) when using pure THF and admitting some air into the reaction flask, or by carrying out the reduction reaction in THF under a pure nitrogen atmosphere (99.9995 %). All of the above experiments suggest that **8** mainly follows from a genuine side-reaction with N$_2$ (Scheme 7). As a result of its coordination to four Mo atoms, the dinitrogen molecule is activated almost to the diazendiide point (see below), and it would be quite interesting to analyse its reactivity. Unfortunately, attempts to prepare compound **8** in a more selective way have been unsuccessful so far, and further synthetic work will be needed in the future before the chemistry of this unusual dinitrogen complex

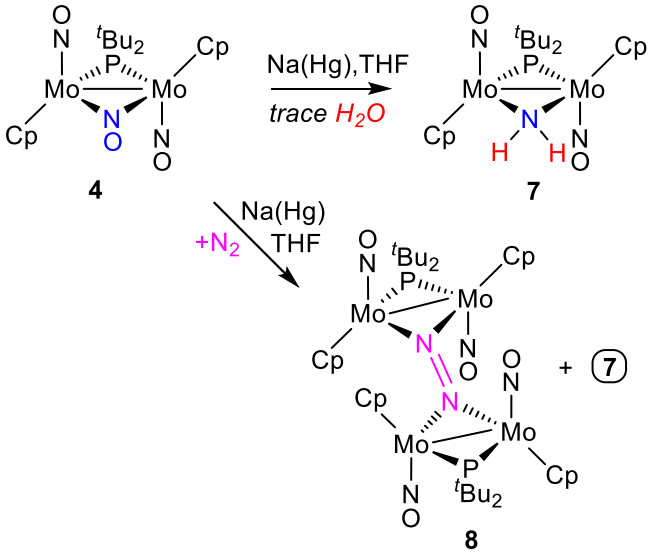

Scheme 7. Reduction reactions of compound **4**.

can be explored in detail. It can be conceived that, as opposed to the multielectron reduction required to transform a bridging nitrosyl into an amide ligand (eq. (1)) [4], the formation of **8** might follow from a side-reaction of the radical anion likely formed in the first electron transfer, which might evolve by releasing the nitroside anion to give a 31-electron dimolybdenum radical (eqs (2) and 3). Direct dimerization of this new and neutral radical would possibly be precluded for steric reasons, but its high electron deficiency would enable it to react even with the poorly donor molecule of dinitrogen (but with good π accepting properties) to give the tetranuclear product **8** (eq. (4)). The nitroside anion is a quite basic species, and likely would be protonated during workup to give free nitroxyl (HNO), this in turn degrading rapidly into N$_2$O and H$_2$O [24].

$$Mo_2(\mu\text{-NO}) + 4e^- + 3H_2O \rightarrow Mo_2(\mu\text{-NH}_2) + 4OH^- \quad (1)$$

$$Mo_2(\mu\text{-NO}) + 1e^- \rightarrow \cdot Mo_2(\mu\text{-NO})^- \quad (2)$$

$$Mo_2(\mu\text{-NO})^- \rightarrow \cdot Mo_2 + NO^- \quad (3)$$

$$2\ \cdot Mo_2 + N_2 \rightarrow Mo_2(\mu_4\text{-N}_{-2})Mo_2 \quad (4)$$

Spectroscopic data for **7** (Table 2 and Experimental section) are comparable to those of its PCy$_2$-bridged analogue, a complex structurally characterized by X-ray diffraction methods [4], and deserve no detailed comments. We just note that the presence of the bridging amide group is denoted by the appearance of a broad resonance at 3.69 ppm corresponding to two H atoms in its ^{1}H NMR spectrum, as well as weak N—H stretching bands at 3354 and 3273 cm^{-1} in its solid-state IR spectrum (Nujol mull).

2.6. Structure of the dinitrogen-bridged complex 8

The molecular structure of **8** in the crystal (Fig. 6 and Table 5) can be derived from two molecules of **4** after removing the bridging nitrosyl ligand and connecting both dimetal units through a dinitrogen molecule in the novel μ$_4$-k^1:k^1:k^1:k^1 fashion. Geometrical parameters within each Mo$_2$ subunit are comparable to those in the parent complex **4**, including the short intermetallic length of ca. 2.89 Å (cf. 2.905(1) Å in **4**), which is consistent with the presence of metal-metal single bonds.

As for the N$_2$ ligand, we first note that the environment around the N atoms is almost perfectly trigonal, and that the corresponding Mo$_2$N planes are rotated from each other by ca. 35°. The Mo-N (ca. 2.07 Å), and N—N distances (1.241(3) Å) in **8** are comparable to those measured in the diazenide-bridged complexes [W$_2$Cp$_2$(μ-k^1:k^1-NNMe)(μ-PCy$_2$)(NO)$_2$] (ca. 2.05 and 1.246(4) Å) [25], and [Mo$_2$Cp$_2$(μ-k^1:k^1-NNPh)(μ-SMe)$_3$] (ca. 2.06 and 1.255(3) Å) [26]. All these N—N lengths are in turn comparable to the reference N—N double bond distances of ca. 1.25 Å measured in free diazenes, and substantially higher than the value of 1.098 Å corresponding to the triple bond in the free N$_2$ molecule [27, 28]. Thus it has to be concluded that we are facing a case of strong activation of the N$_2$ molecule [27], with large electron transfer from the metal atoms to the π^*(N—N) orbital to effectively render almost a coordinated diazendiide (N_2^{2-}) ligand. The fact that the Mo$_2$(μ-N) planes in **8** are rotated from each other, then departing from the coplanar arrangement optimizing orbital overlaps with a N_2^{2-} ligand, might have a steric origin. We finally stress that, although many different coordination modes have been identified so far for bridging N$_2$ ligands [29], compound **8** represents the first example in its class (Fig. 7). All previous examples of complexes having N$_2$ ligands interacting with four metal atoms belong to the type μ$_4$-k^1:η^2:k^1:η^2, and typically involve weak η^2 interactions with alkali metal cations [30].

The IR and ^{31}P NMR spectra for **8** in solution are comparable to the ones for the amide-bridged complex **7**, as expected from the presence of similar Mo$_2$Cp$_2$(μ-N)(μ-PR$_2$)(NO)$_2$ fragments in both cases. Moreover, the ^{1}H NMR spectrum of the complex denotes the chemical equivalence of all Cp and ^{t}Bu$_2$ groups of the molecule, in full agreement with the

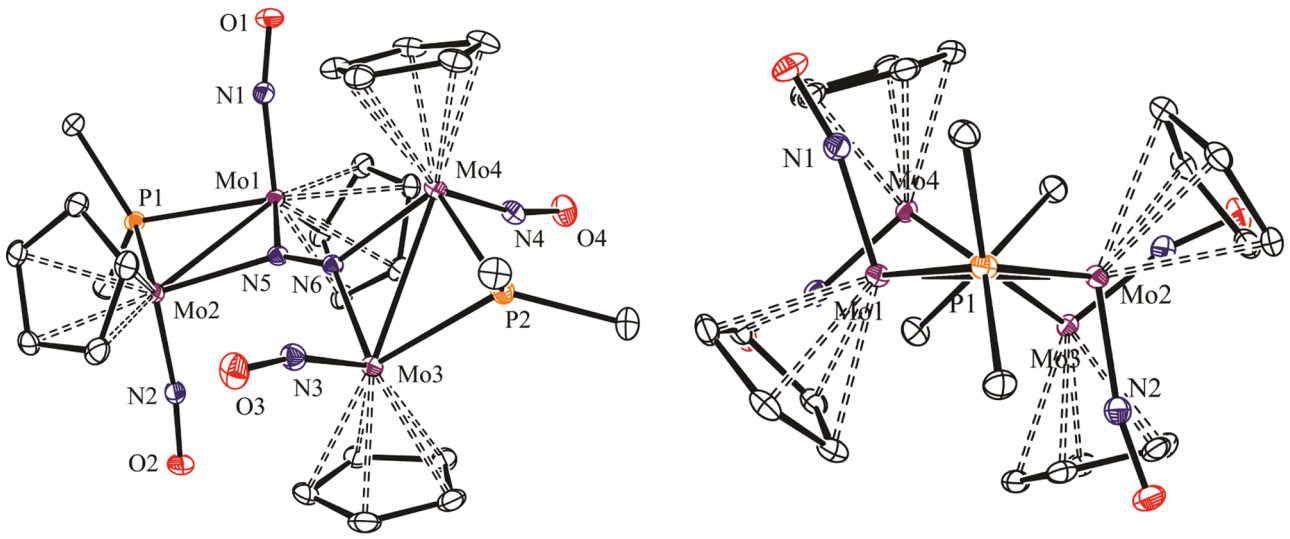

Fig. 6. ORTEP diagram (30 % probability) of compound **8**, with ^{t}Bu groups (except their C^{1} atoms) and H atoms omitted for clarity. On the right, a view of the molecule along the N5-N6 vector.

Table 5
Selected bond lengths (Å) and angles (°) for compound **8**.

Mo1-Mo	2.8901(3)	Mo1-P1-Mo2	72.20(2)
Mo1-P1	2.4462(7)	Mo1-N5-Mo2	88.4(1)
Mo2-P1	2.4589(7)	P1-Mo1-N1	96.10(8)
Mo1-N5	2.073(2)	P1-Mo1-N5	99.74(6)
Mo2-N5	2.073(2)	P1-Mo2-N2	96.65(8)
Mo1-N1	1.781(2)	P1-Mo2-N5	99.32(6)
Mo2-N2	1.783(2)	Mo1-N5-N6	135.4(2)
N5-N6	1.241(3)	Mo2-N5-N6	136.2(2)
N1-O1	1.215(3)	Mo1-N1-O1	166.7(2)
N2-O2	1.218(3)	Mo2-N2-O2	168.5(2)

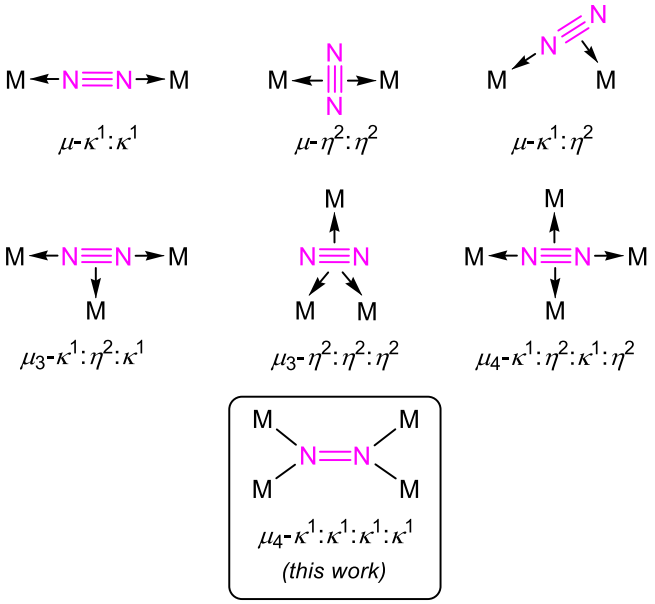

Fig. 7. Coordination modes of the bridging N_2 ligand, depicted as following from weak dinitrogen activation for simplicity, except for the coordination mode found in **8** (strong activation, see text).

structure found in the crystal discussed above, where all four MoCp(NO) fragments are related by approximate symmetry elements (C_2 axis). As noted above, compound **8** displays a deep purple colour, in contrast to the yellow-coloured **7**. This difference can be associated to the presence of a bridging dinitrogen ligand in the former, that would provide the molecule with a low energy LUMO, likely with high π^*(N—N) antibonding character, that would enable the absorption in the low-energy region of the visible spectrum.

3. Conclusions

The trinitrosyl complex $[Mo_2Cp_2(\mu\text{-}P^tBu_2)(\mu\text{-}NO)(NO)_2]$ (**4**) can be efficiently prepared in a three-step procedure starting with the hydride complex $[Mo_2Cp_2(\mu\text{-}H)(\mu\text{-}P^tBu_2)(CO)_4]$, which is first dehydrogenated through reaction with a strong acid to give the unsaturated cation $[Mo_2Cp_2(\mu\text{-}P^tBu_2)(CO)_4]^+$ (Mo=Mo), followed by reaction with NO to give the dinitrosyl cation $[Mo_2Cp_2(\mu\text{-}P^tBu_2)(CO)_2(NO)_2]^+$, this finally rendering the targeted trinitrosyl complex upon reaction with a soluble nitrite salt that induces further decarbonylation and nitrosylation processes. Experimental and theoretical studies indicate that the above unsaturated tetracarbonyl intermediate displays an asymmetric transoid arrangement of the $MoCp(CO)_2$ fragments of the molecule, and that this would be also the case of related cations with different PR_2 groups which were previously assumed to have a cisoid arrangement of their metal fragments. The structural data for **4** are comparable to those of its PCy_2-bridged analogue, particularly as concerning the pyramidalization degree of the bridging NO, therefore a similar N—O activation chemistry could be anticipated. Indeed, the protonation, deoxygenation with phosphites and reduction with active-metal amalgams proceeded analogously to give nitroxyl-, phosphoraniminate-, and amide-bridged derivatives, respectively. However, the latter reaction also yielded an unexpected side product in the presence of nitrogen, fully identified as $[Mo_4Cp_4(\mu\text{-}P^tBu_2)_2(\mu_4\text{-}k^1\text{:}k^1\text{:}k^1\text{:}k^1\text{-}N_2)(NO)_4]$, with a dinitrogen molecule displaying a novel μ_4 coordination mode and involved in strong interaction with the metal atoms that takes it almost to the diazendiide (N_2^{2-}) limit, as judged from the experimental N—N separation of 1.241(3) Å, a value characteristic of conventional $N = N$ double bonds. This product might possibly follow from nitroside (NO^-) release from the anionic radical that would be formed upon the first electron uptake of compound **4**, to give a new radical, unsaturated and neutral, able to interact with the dinitrogen molecule.

4. Experimental

4.1. General procedures and starting materials

All manipulations and reactions were carried out under an argon (99.995 %) atmosphere using standard Schlenk techniques unless otherwise indicated. Solvents were purified according to literature procedures, and distilled prior to use [31]. All reagents were obtained from commercial suppliers and used as received. Petroleum ether refers to that fraction distilling in the range 338–343 K. Filtrations were carried out through diatomaceous earth unless otherwise stated. Chromatographic separations were performed using jacketed columns cooled by tap water (ca. 288 K) or by a closed 2-propanol circuit kept at the desired temperature with a cryostat. Commercial aluminium oxide (activity I, 70–290 mesh) was degassed under vacuum prior to use. The latter was mixed under argon with the appropriate amount of water to reach activity IV. Silica gel (230–400 mesh) was used as received. Photochemical experiments were performed using jacketed Pyrex Schlenk tubes cooled by a closed 2-propanol circuit kept at the desired temperature with a cryostat; a 400 W medium-pressure mercury lamp placed ca. 1 cm away from the Schlenk tube was used for these experiments. IR stretching frequencies of NO and CO ligands were usually measured in solution (using CaF_2 windows), are referred to as ν(XO) ($X = N$, C), and are given in wave number units (cm^{-1}). Nuclear magnetic resonance (NMR) spectra were routinely recorded at 295 K unless otherwise stated. Chemical shifts (δ) are given in ppm, relative to internal tetramethylsilane (^1H, ^{13}C), or external 85 % aqueous H_3PO_4 solutions (^{31}P). Coupling constants (J) are given in hertz.

4.2. Improved preparation of [$Mo_2Cp_2(\mu\text{-}H)(\mu\text{-}P^tBu_2)(CO)_4$] (1)

Neat PH^tBu_2 (270 μL, 1.513 mmol) was added to a toluene solution (20 mL) of [$Mo_2Cp_2(CO)_6$] (0.600 g, 1.224 mmol), and the mixture was refluxed for 4.5 h with a gentle argon purge to give a red solution. The solvent was then removed under vacuum, the residue was extracted with dichloromethane/petroleum ether (1/4), and the extracts were chromatographed on silica gel at 288 K. Elution with dichloromethane/petroleum ether (1/2) gave a red fraction yielding, upon removal of solvents, compound **1** as a red solid (0.545 g, 77 %). ν(CO) (CH_2Cl_2): 1948 (w, sh), 1929 (vs), 1854 (m). Other spectroscopic data for this complex were identical to those reported previously in the literature [7].

4.3. Preparation of [$Mo_2Cp_2(\mu\text{-}P^tBu_2)(CO)_4$][$BF_4$] (2-$BF_4$)

Neat $HBF_4{\cdot}OEt_2$ (90 μL, 0.662 mmol) was added to a dichloromethane solution (20 mL) of compound **1** (0.250 g, 0.431 mmol), and the mixture was stirred at room temperature for 30 min to give a black solution that was filtered. The solvent was then removed from the filtrate under vacuum, the residue was washed with diethyl ether (4 × 10 mL), and dried under vacuum to give compound **2-BF_4** as a black powder (0.260 g, 91 %). Anal Calcd. for $C_{22}H_{28}BF_4Mo_2O_4P$: C, 39.67; H, 4.24. Found: 39.76; H, 4.21. ^1H NMR (300.13 MHz, CD_2Cl_2): δ 5.97 (s, 10H, Cp), 1.35 (d, J_{HP} = 16, 18H, ^{t}Bu). $^{13}C\{^1H\}$ NMR (100.63 MHz, CD_2Cl_2): δ 229.0 (br, MoCO), 97.5 (s, Cp), 45.9 [d, J_{CP} = 11, $C^1(^t$Bu)], 33.5 [d, J_{CP} = 4, $C^2(^t$Bu)].

4.4. Preparation of [$Mo_2Cp_2(\mu\text{-}P^tBu_2)(CO)_4$][$BAr'_4$] (2-$BAr'_4$)

Solid Na(BAr'_4) (0.053 g, 0.060 mmol; Ar' = 3,5-$C_6H_3(CF_3)_2$) was added to a solution of compound **2-BF_4** (0.035 g, 0.053 mmol) in dichloromethane (10 mL), and the mixture was stirred at room temperature for 5 min, then filtered. Removal of the solvent from the filtrate under vacuum and washing of the residue with petroleum ether (3 × 5 mL) gave compound **2-BAr'$_4$** as a black solid (0.055 g, 72 %). The crystals used in the X-ray study of this compound were grown by the slow diffusion of layers of toluene and petroleum ether into a concentrated dichloromethane solution of the complex at 253 K. Anal. Calcd for $C_{54}H_{40}BF_{24}Mo_2O_4P$: C, 44.96; H, 2.79. Found: C, 45.04; H, 2.75. ^1H NMR (300.13 MHz, CD_2Cl_2): δ 7.72 (s, br, 8H, Ar'), 7.56 (s, 4H, Ar'), 5.91 (s, 10H, Cp), 1.32 (d, J_{HP} = 16, 18H, ^{t}Bu). $^{13}C\{^1H\}$ NMR (100.63 MHz, CD_2Cl_2): δ 229.5 (br, MoCO), 97.5 (s, Cp), 46.0 [d, J_{CP} = 11, $C^1(^t$Bu)], 33.5 [d, J_{CP} = 4, $C^2(^t$Bu)]. *Low temperature NMR data* (only resonances for the cation given): $^{13}C\{^1H\}$ NMR (100.63 MHz, CD_2Cl_2, 203 K): δ 242.7 (s, MoCO), 228.4 (s, J_{CP} = 44, MoCO), 227.1 (d, J_{CP} = 6, MoCO), 221.2 (s, MoCO), 100.5, 94.5 (2 s, Cp), 46.8 [d, J_{CP} = 13, $C^1(^t$Bu)], 44.1 [d, J_{CP} = 10, $C^1(^t$Bu)], 33.7 [d, J_{CP} = 7, $C^2(^t$Bu)], 32.6 [s, $C^2(^t$Bu)]. ^1H NMR (400.13 MHz, CD_2Cl_2, 253 K): δ 5.93 (s, 10H, Cp), 1.31 (d, J_{HP} = 16, 18H, ^{t}Bu). ^1H NMR (400.13 MHz, CD_2Cl_2, 233 K): δ 5.94 (s, br, 10H, Cp), 1.30 (s, br, 18H, ^{t}Bu). ^1H NMR (400.13 MHz, CD_2Cl_2, 213 K): δ 6.04, 5.87 (2 s, 2 × 5H, Cp), 1.36 (d, br, J_{HP} = 17, 9H, ^{t}Bu), 1.22 (d, br, J_{HP} = 16, 9H, ^{t}Bu). Coalescence temperature of Cp resonances: T_c = 230 K.

4.5. Preparation of [$Mo_2Cp_2(\mu\text{-}P^tBu_2)(CO)_2(NO)_2$][$BF_4$] (3-$BF_4$)

Nitric oxide (5 % in N_2) was gently bubbled through an stirred 1,2-dichloroethane solution (15 mL) of compound **2-BF_4** (0.260 g, 0.390 mmol) for 45 min at room temperature, to give an orange solution which was filtered. Removal of the solvent from the filtrate under vacuum yielded essentially pure compound **3-BF_4** (0.220 g, 84 %), which was used without further purification. ^1H NMR (300.13 MHz, CD_2Cl_2): δ 5.97 (s, 10H, Cp), 1.34 (d, J_{HP} = 16, 18H, ^{t}Bu).

4.6. Preparation of [$Mo_2Cp_2(\mu\text{-}P^tBu_2)(CO)_2(NO)_2$][$BAr'_4$] (3-$BAr'_4$)

Solid Na(BAr_4) (0.100 g, 0.113 mmol) was added to a dichloromethane solution (10 mL) of crude compound **3-BF_4** (0.075 g, 0.112 mmol), and the mixture was stirred for 10 min, then filtered. Removal of the solvent under vacuum and washing of the residue with petroleum ether (5 mL) gave essentially pure compound **3-BAr'$_4$** as a yellow solid (0.140 g, 86 %), ready for further use. Additional purification can be achieved upon chromatography on alumina at 288 K. To this purpose, the crude product was dissolved in dichloromethane/petroleum ether (1/1), introduced into the column, and eluted with neat dichloromethane to give, after removal of the solvent, compound **3-BAr'$_4$** as a yellow solid (0.055 g, 34 %). Anal. Calcd for $C_{52}H_{40}BF_{24}Mo_2N_2O_4P$: C, 43.18; H, 2.79; N, 1.94. Found: C, 43.10; H, 2.88; N, 2.03. ^1H NMR (400.13 MHz, CD_2Cl_2): δ 7.72 (s, br, 8H, Ar'), 7.56 (s, 4H, Ar'), 5.87 (s, 10H, Cp), 1.33 (d, J_{HP} = 16, 18H, ^{t}Bu). $^{13}C\{^1H\}$ NMR (100.63 MHz, CD_2Cl_2): δ 220.3 (d, J_{CP} = 21, MoCO), 162.1 [q, J_{CB} = 50, C^1(Ar')], 135.2 [s, C^2(Ar')], 129.3 [qq, J_{CF} = 32, J_{CB} = 3, C^3(Ar')], 125.2 (q, J_{CF} = 272, CF_3), 117.9 [spt, J_{CF} = 4, C^4(Ar')], 98.5 (s, Cp), 47.9 [d, J_{CP} = 7, $C^1(^t$Bu)], 33.2 [d, J_{CP} = 3, $C^2(^t$Bu)].

4.7. Preparation of [$Mo_2Cp_2(\mu\text{-}P^tBu_2)(\mu\text{-}NO)(NO)_2$] (4)

Solid [PPN]NO_2 (0.304 g, 0.520 mmol; PPN = $N(PPh_3)_2$) was added to a dichloromethane solution (15 mL) of compound **3-BF_4** (0.290 g, 0.433 mmol), and the mixture was stirred at room temperature for 3 min to give a blue solution. After removal of the solvent under vacuum, the residue was extracted with dichloromethane/petroleum ether (1/2), and the extracts chromatographed on alumina at 288 K. Elution with dichloromethane/petroleum ether (1/1) gave a blue fraction yielding, upon removal of solvents, compound **4** as a dark blue microcrystalline solid (0.180 g, 75 %). The crystals used in the X-ray study of **4** were grown by the slow diffusion of a layer of petroleum ether into a concentrated toluene solution of the complex at 253 K. Anal. Calcd for $C_{18}H_{28}Mo_2N_3O_3P$: C, 38.79; H, 5.06; N, 7.54. Found: C, 38.49; H, 5.23; N, 7.06. ν(NO) (KBr disk): 1583 (vs), 1407 (m). ^1H NMR (400.13 MHz, CD_2Cl_2): δ 5.76 (s, 10H, Cp), 1.40 (d, J_{HP} = 14, 18H, ^{t}Bu). $^{13}C\{^1H\}$ NMR (100.63 MHz, CD_2Cl_2): δ 100.4 (s, Cp), 43.2 [d, J_{CP} = 9, $C^1(^t$Bu)], 33.1 [d, J_{CP} = 5, $C^2(^t$Bu)].

4.8. Preparation of cis-[$Mo_2Cp_2(\mu\text{-}P^tBu_2)(\mu\text{-}NO)(NO)_2$] (cis-4)

A toluene solution (8 mL) of compound **4** (0.035 g, 0.063 mmol) was irradiated at 263 K with visible-UV light for 1.5 h to give a greenish solution containing a ca. 2:1 mixture of ***cis*-4** and **4** (as determined by ^{31}P NMR spectroscopy) which was filtered. Removal of solvent under vacuum from the filtrate gave a blue residue (0.022 g, 63 %). The latter was then dissolved in dichloromethane/petroleum ether (1/2) and chromatographed on alumina at 253 K. Elution with the same solvent mixture gave a blue-greenish fraction that was collected in three portions shown (by ^{31}P NMR, after removal of solvents) to contain ***cis*-4**/**4** mixtures in ca. 1:8, 1:1, and 8:1 ratios. The latter fraction (0.005 g, ca. 14 %) was used for recording the spectra of isomer ***cis*-4**. ^1H NMR (300.13 MHz, CD_2Cl_2): δ 5.59 (s, 10H, Cp), 1.78 (d, $J_{HP} = 15$, 9H, ^{t}Bu), 1.16 (d, br, $J_{HP} = 13$, 9H, ^{t}Bu).

4.9. Preparation of [$Mo_2Cp_2(\mu\text{-}P^tBu_2)(\mu\text{-}\kappa^1;\eta^2\text{-}HNO)(NO)_2$] (5-$BF_4$)

Neat $HBF_4{\cdot}OEt_2$ (11 μL, 0.081 mmol) was added to a dichloromethane solution (10 mL) of compound **4** (0.040 g, 0.072 mmol), and the mixture was stirred at room temperature for 5 min to give a pink solution which was filtered. Workup as described for **2-BF_4** gave compound **5-BF_4** as a pink solid shown (by NMR) to exist in CD_2Cl_2 solution as an equilibrium mixture of isomers **5-BF_4** and **5′-BF_4** in a ca. 5/1 ratio. The crystals used in the X-ray study of **5-BF_4** were grown by the slow diffusion of a layer of petroleum ether into a dichloromethane solution of the complex at 253 K. Anal. Calcd for $C_{18}H_{29}BF_4Mo_2N_3O_3P$: C, 33.51; H, 4.53; N, 6.51. Found: C, 33.20; H, 4.68; N, 6.29. *Data for isomer **5-BF_4***: ^1H NMR (400.13 MHz, CD_2Cl_2): δ 12.21 (s, br, 1H, NH), 6.22, 5.95 (2 s, 2 × 5H, Cp), 1.57 (d, $J_{HP} = 16$, 9H, ^{t}Bu), 1.4 (vbr, 9H, ^{t}Bu). $^{13}C\{^1H\}$ NMR (100.63 MHz, CD_2Cl_2): δ 103.2, 103.2 (2 s, Cp), 49.5, 47.3 [2 s, $C^1(^tBu)$], 34.2 [d, $J_{CP} = 3$, $C^2(^tBu)$], 32.5 (vbr, $C^2(^tBu)$. *Data for isomer **5′-BF_4***: ^1H NMR (300.13 MHz, CD_2Cl_2): δ 13.15 (s, br, 1H, NH), 6.45, 6.34 (2 s, 2 × 5H, Cp), 1.64 (d, $J_{HP} = 16$, 9H, ^{t}Bu), 1.24 (d, br, $J_{HP} = 17$, 9H, ^{t}Bu). $^{13}C\{^1H\}$ NMR (100.63 MHz, CD_2Cl_2): δ 104.4, 102.9 (2 s, Cp).

4.10. Preparation of [$Mo_2Cp_2(\mu\text{-}P^tBu_2)\{\mu\text{-}NP(OEt)_3\}(NO)_2$] (6)

Neat $P(OEt)_3$ (370 μL, 2.15 mmol) was added to a toluene solution (12 mL) of compound **4** (0.040 g, 0.072 mmol) in a Schlenk tube equipped with a Young's valve. After closing the valve, the mixture was heated at 398 K for 17 h to give a brown solution. The solvent was then removed under vacuum, the residue was dissolved in dichloromethane/petroleum ether (1/3), and chromatographed on alumina at 253 K. Elution with dichloromethane/petroleum ether (1/1) gave a yellow fraction yielding, after removal of solvents, compound **6** as a yellow solid (0.020 g, 39 %). Anal. Calcd for $C_{24}H_{43}Mo_2N_3O_5P_2$: C, 40.75; H, 6.13; N, 5.94. Found: C, 40.51; H, 6.45; N, 5.86. ^1H NMR (400.13 MHz, C_6D_6): δ 5.75 (s, 10H, Cp), 3.85, 3.60 (2 m, 2 × 3H, OCH_2), 1.44 (d, $J_{HP} = 13$, 18H, ^{t}Bu), 1.04 (t, $J_{HH} = 7$, 9H, CH_3). $^{13}C\{^1H\}$ NMR (100.63 MHz, C_6D_6): δ 96.8 (s, Cp), 63.3 (d, $J_{CP} = 5$, OCH_2), 43.5 [d, $J_{CP} = 10$, $C^1(^tBu)$], 33.9 [d, $J_{CP} = 4$, $C^2(^tBu)$], 16.1 (d, $J_{CP} = 8$, CH_3).

4.11. Preparation of [$Mo_2Cp_2(\mu\text{-}P^tBu_2)(\mu\text{-}NH_2)(NO)_2$] (7)

Degassed water (50 μL), and then an excess of 0.5 % sodium amalgam (ca. 1 mL), were added to a tetrahydrofuran solution (10 mL) of compound **4** (0.040 g, 0.072 mmol), and the mixture was vigorously stirred for 10 min at room temperature to give a yellow solution which was transferred using a canula to a second flask to discard the amalgam. After removal of the solvent under vacuum from that solution, the residue was dissolved in dichloromethane/petroleum ether (1/2) and chromatographed on alumina at 253 K. Elution with the same solvent mixture gave usually a faint purple fraction containing very small amounts of complex **8**. Elution with neat dichloromethane gave a major yellow fraction yielding, after removal of solvents, compound **7** as a yellow solid (0.025 g, 64 %). Anal. Calcd for $C_{18}H_{30}Mo_2N_3O_2P$: C, 39.79; H, 5.57; N, 7.73. Found: C, 40.06; H, 5.76; N, 7.65. IR (Nujol mull): 3354 (w, N—H), 3273 (w, N—H), 1554 (m, N—O), 1534 (s, N—O). ^1H NMR (400.13 MHz, CD_2Cl_2): δ 5.73 (s, 10H, Cp), 3.69 (s, br, 2H, NH_2), 1.34 (d, $J_{HP} = 14$, 18H, ^{t}Bu). $^{13}C\{^1H\}$ NMR (100.63 MHz, CD_2Cl_2): δ 96.7 (s, Cp), 43.3 [d, $J_{CP} = 10$, $C^1(^tBu)$], 33.8 [d, $J_{CP} = 4$, $C^2(^tBu)$].

4.12. Preparation of [$Mo_4Cp_4(\mu\text{-}P^tBu_2)_2(\mu\text{-}\kappa^1{:}\kappa^1{:}\kappa^1{:}\kappa^1\text{-}N_2)(NO)_4$] (8)

An excess of 0.5 % sodium amalgam (ca. 1 mL) was added to a tetrahydrofuran solution (8 mL) of compound **4** (0.040 g, 0.072 mmol), previously saturated with nitrogen (99.9995 %) at 273 K, and the mixture was gently stirred for 15 min at that temperature under a nitrogen atmosphere to give a dark purple solution shown (by ^{31}P NMR) to contain a mixture of compounds **7** and **8** in a ratio of ca. 5:1. Workup under argon as described for **7** gave first the minor compound **8** as a dark purple solid (0.004 g, 10 %), then the major compound **7** as a yellow solid (0.020 g, 50 %). The crystals used in the X-ray study of **8** were grown by the slow diffusion of layers of toluene and petroleum ether into a concentrated dichloromethane solution of the complex at 253 K. *Data for compound **8***: Anal. Calcd for $C_{36}H_{56}Mo_4N_6O_4P_2$: C, 39.94; H, 5.21; N, 7.76. Found: C, 39.65; H, 4.98; N, 7.41. ^1H NMR (300.13 MHz, CD_2Cl_2): δ 5.64 (s, 10H, Cp), 1.52 (d, $J_{HP} = 14$, ^{t}Bu).

4.13. X-Ray structure determination of compounds 2-BAr′$_4$, 4, and 8

Data collection for these compounds was performed using Cu Kα radiation at ca. 100 K (**2-BAr′$_4$** and **8**) or 150 K (**4**) on *Rigaku XtaLAB Synergy-S Flow* or *Oxford Diffraction Xcalibur Nova* diffractometers, respectively. Images were collected with the ω scans or oscillation methods, respectively. Data collection strategy was calculated with the program *CrysAlis Pro CCD* [32], and data reduction and cell refinements were performed with the program *CrysAlis Pro RED* [32]. In all cases an empirical absorption correction was applied using the SCALE3 ABSPACK algorithm as implemented in the above program. Using the program suite WinGX [33], the structures were solved using either *Superflip* (**2** and **8**) [34] or SHELXL2018/3 (**4**) [35], and refined with full-matrix least squares on F^2 using SHELXL2018/3. In general, all non-hydrogen atoms were refined anisotropically, except for atoms involved in disorder, and all hydrogen atoms were geometrically placed and refined using a riding model. As for compound **2-BAr′$_4$**, three CF_3 groups in the anion were disordered over two sites each, satisfactorily refined with 0.5/0.5 occupancies. The structure of the cation displayed no apparent disorder, but two anomalously strong residual peaks of ca. 9 electrons remained in the final difference map, each of them close to a Mo atom and separated from each other by 2.837 Å, almost the same distance as the intermetallic separation in the cation (2.8283(7) Å). This causes A-level alerts in the corresponding checkcif file. As there was no crystallographic evidence for twinning in the crystal, nor of absorption problems, we interpret this high residuals as due to a whole-body disorder of the cation over two sites with distinct occupancies, with the (not modelled) minor site having an occupancy of around 15 %. In compound **4**, one of the Cp rings displayed incipient disorder that could not be properly modelled. Compound **8** crystallized with a molecule of dichloromethane, which could be refined in a conventional way. Crystal data and refinement values for these compounds are collected in Table S1 of the supplementary material.

4.14. X-Ray structure determination of compound 5-BF_4

Data collection for this compound was performed at ca. 100 K on a *Bruker D8 Venture Photon III 14 k-geometry* diffractometer, using Mo K_α radiation. The software APEX3 [36] was used for collecting frames with the ω/ϕ scan measurement method. The SAINT V8.40B software was used for data reduction [37], and a multi-scan absorption correction was applied with SADABS-2016/2 [38]. Structure solution and refinements

were performed as described for **4**. In this case, the N-bound H atom of the cation was located in the Fourier maps and refined isotropically.

4.15. Computational details

All DFT calculations were carried out using the GAUSSIAN16 package [39], and the M06L functional [40]. A pruned numerical integration grid (99,590) was used for all the calculations via the keyword Int=Ultrafine together with the empirical dispersion correction from Grimme and co-workers via the keyword GD3 [41]. SDD effective core potentials and its associated basis set were used for Mo atoms [42]. The light elements (P, N, O, C and H) were described with the 6–31G* basis [43]. Geometry optimizations were performed under no symmetry restrictions, using initial coordinates derived from X-ray data. Frequency analyses were performed for all the stationary points to ensure that a minimum structure with no imaginary frequencies was achieved in each case.

CRediT authorship contribution statement

M. Angeles Alvarez: Writing – review & editing, Investigation, Data curation. **M. Esther García:** Writing – review & editing, Supervision, Methodology, Conceptualization. **Daniel García-Vivó:** Writing – review & editing, Writing – original draft, Visualization, Software, Investigation, Data curation, Conceptualization. **Ana M. Guerra:** Writing – review & editing, Visualization, Investigation, Data curation. **Miguel A. Ruiz:** Writing – review & editing, Writing – original draft, Supervision, Resources, Project administration, Methodology, Investigation, Funding acquisition, Data curation, Conceptualization.

Declaration of competing interest

The authors declare that they have no known competing financial interests or personal relationships that could have appeared to influence the work reported in this paper.

Data availability

Data will be made available on request.

Acknowledgment

We thank the MICIU and AEI of Spain and FEDER for financial support (Project PGC2021–123964NB-I00), the SCBI of the Universidad de Málaga, Spain, for access to computing facilities, and the X-Ray unit of the Universidad de Santiago de Compostela, Spain, for acquisition of diffraction data.

Supplementary materials

Supplementary material associated with this article can be found, in the online version, at doi:10.1016/j.jorganchem.2024.123375.

References

[1] a)G.B. Richter-Addo, P. Legzdins, Metal Nitrosyls, Oxford University Press, Oxford, U. K., 1992.
b)Nitrosyl Complexes in Inorganic Chemistry, Biochemistry and Medicine, D. M. P. Mingos, (Ed.), Struct. Bond. 2014, Vol 153 and 154.

[2] a) For some recent reviews, see L. Han, S. Cai, M. Gao, J. Hasegawa, P. Wang, J. Zhang, L. Shi, D. Zhang, Selective catalytic reduction of NO_x with NH_3 by using novel catalysts: state of the art and future prospects, Chem. Rev. 119 (2019) 10916, https://doi.org/10.1021/acs.chemrev.9b00202;
b) J.K. Lai, I.E. Wachs, A perspective on the selective catalytic reduction (SCR) of NO with NH_3 by supported V_2O_5–WO_3/TiO_2 catalysts, ACS Catal 8 (2018) 6537, https://doi.org/10.1021/acscatal.8b01357;
c) Y. Liu, J. Zhao, J.-M. Lee, Conventional and new materials for selective catalytic reduction (SCR) of NO_x, ChemCatChem 10 (2018) 1499, https://doi.org/10.1002/cctc.201701414.

[3] a) For previous work of other groups on N-O bond cleavage of nitrosyl ligands at binuclear complexes, see Z. Cai, W. Tao, C.E. Moore, S. Zhang, C.R. Wade, Direct NO Reduction by a biomimetic Iron(II) Pyrazolate MOF, Angew. Chem. Int. Ed. 60 (2021) 21221, https://doi.org/10.1002/anie.202108095;
b) Y. Arikawa, Y. Otsubo, H. Fujino, S. Horiuchi, E. Sakuda, K. Umakoshi, Nitrite reduction cycle on a dinuclear ruthenium complex producing ammonia, J. Am. Chem. Soc. 140 (2018) 842, https://doi.org/10.1021/jacs.7b12020;
c) Y. Arikawa, J. Hiura, C. Tsuchii, M. Kodama, N. Matsumoto, K. Umakoshi, Synthetic NO reduction cycle on a bis(pyrazolato)-bridged dinuclear ruthenium complex including photo-induced transformation, Dalton Trans 47 (2018) 7399, https://doi.org/10.1039/C8DT01208C;
d) T. Suzuki, H. Tanaka, Y. Shiota, P.K. Sajith, Y. Arikawa, K. Yoshizawa, Proton-Assisted Mechanism of NO Reduction on a Dinuclear Ruthenium Complex, Inorg. Chem. 54 (2015) 7181, https://doi.org/10.1021/acs.inorgchem.5b00394;
e) Y. Arikawa, T. Asayama, M. Moriguchi, S. Agari, M. Onishi, Reversible N–N Coupling of NO Ligands on Dinuclear Ruthenium Complexes and Subsequent N_2O Evolution: relevance to Nitric Oxide Reductase, J. Am. Chem. Soc. 129 (2007) 14160, https://doi.org/10.1021/ja0763504;
f) P. Legzdins, M.A. Young, R.J. Batchelor, F.W.B. Einstein, Spontaneous isomerization of symmetric M(μ-NO)$_2$M Linkages to (ON)M=N=M=O groupings, J. Am. Chem. Soc. 117 (1995) 8798, https://doi.org/10.1021/ja00139a013.

[4] a) M.A. Alvarez, M.E. García, D. García-Vivó, A. Ramos, M.A. Ruiz, A. Toyos, N-O bond activation and cleavage reactions of the nitrosyl-bridged complexes [M_2Cp_2(μ-PCy_2)(μ-NO)(NO)$_2$] (M = Mo, W), Inorg. Chem. 57 (2018) 15314, https://doi.org/10.1021/acs.inorgchem.8b02647;
b) M.A. Alvarez, M.E. García, D. García-Vivó, A. Ramos, M.A. Ruiz, A. Toyos, Mild N-O bond cleavage reactions of a Pyramidalized Nitrosyl ligand bridging a Dimolybdenum center, Inorg. Chem. 54 (2015) 10536, https://doi.org/10.1021/acs.inorgchem.5b02292.

[5] M.A. Alvarez, M.E. García, D. García-Vivó, A.M. Guerra, M.A. Ruiz, Chemistry of a Nitrosyl Ligand *k*:*η*-bridging a Ditungsten center: rearrangement and N-O Bond cleavage reactions, Inorg. Chem. 61 (2022) 14929, https://doi.org/10.1021/acs.inorgchem.2c02216.

[6] M.A. Alvarez, M.E. García, D. García-Vivó, A.M. Guerra, M.A. Ruiz, C=N and N=O bond cleavages of acetonitrile and Nitrosyl ligands at a Dimolybdenum center to render Ethylidyne and Acetamidinate ligands, Inorg. Chem. 63 (2024) 3207, https://doi.org/10.1021/acs.inorgchem.3c03697.

[7] R.A. Jones, S.T. Schwab, A.L. Stuart, B.R. Whittlesey, T.C. Wright, Synthesis of dinuclear phosphido or arsenido bridged complexes of molybdenum via reaction of secondary phosphines or arsines with [Mo(η^5-C_5H_5)(CO)$_3$]$_2$: x-ray structures of {[Mo(η^5-C_5H_5)(CO)$_2$]$_2$(μ-H)(μ-ER_2)} (E = P, R= t-Bu; or E = As, R = Me), Polyhedron 4 (1985) 1689, https://doi.org/10.1016/S0277-5387(00)84160-1.

[8] We have improved the yield of this complex (from 45 to 77%) by reducing the relative amount of phosphine used in the reaction (from 2 to ca 1.2 equiv), and by using chromatography instead of crystallization to isolate the product (see the experimental section).

[9] M.A. Alvarez, M.E. García, D. García-Vivó, M.A. Ruiz, M.F. Vega, Synthesis and reactivity of the triply bonded binuclear anion [W_2(η^5-C_5H_5)$_2$(μ-PCy_2)(μ-CO)$_2$]$^-$: tungsten makes a difference, Organometallics 29 (2010) 512, https://doi.org/10.1021/om9010005, and references therein.

[10] R.D. Adams, D.M. Collins, F.A. Cotton, Molecular structures and barriers to internal rotation in bis (.eta.5-cyclopentadienyl)hexacarbonylditungsten and its molybdenum analog, Inorg. Chem. 13 (1974) 1086, https://doi.org/10.1021/ic50135a015.

[11] A search at the Cambridge Crystallographic Data Centre database (updated March 2024) on binuclear Mo or W organometallic complexes bearing metal-metal double bonds yielded some 160 structures, most of them with intermetallic distances in the range of 2.55-2.80 Å, with a mean value of 2.66 Å.

[12] R.H. Crabtree, M. Lavin, Structural analysis of the semibridging carbonyl, Inorg. Chem. 25 (1986) 805, https://doi.org/10.1021/ic00226a016.

[13] P.S. Braterman, Metal Carbonyl Spectra, Academic Press, London, UK, 1975.

[14] Two-bond couplings involving P atoms ($^2J_{PX}$) in metal complexes increase algebraically with the P-M-X angle, and therefore are quite sensitive to the relative positioning of P and X. Their absolute values for piano-stool complexes of type $MCpPXL_2$ usually follow the order $|^2J_{cis}|_> |^2J_{trans}|$. See, for instance, reference 15, and also B. Wrackmeyer, H.G. Alt, H.E. Maisel, Ein- und zwei-dimensionale Multikern NMR-Spektroskopie an den isomeren Halbsandwich-Komplexen *cis*- und *trans*-[(η^5-C_5H_5)W(CO)$_2$(H)PMe_3], J. Organomet. Chem. 399 (1990) 125, https://doi.org/10.1016/0022-328X(90)80090-M.

[15] C.J. Jameson, in Phosphorus-31 NMR Spectroscopy in Stereochemical Analysis, J. G. Verkade, L.D. Quin, Eds., VCH, Deerfield Beach, FL, 1987, Chapter 6.

[16] According to the modified Eyring equation $DG\#Tc = 19.14Tc[9.97 + \log(Tc/\triangle\nu)]$ (J/mol). See: H. Günter, NMR Spectroscopy, John Wiley, Chichester, UK, 1980, p 243.

[17] Compound [Mo2Cp2(μ-PPh2)(CO)2(NO)2](BF4) was prepared previously by us through the reaction of the nitrosyl complex [Mo2Cp2(μ-PPh2)(CO)3(NO)] with [NO]BF4, and it displays similar spectroscopic properties The structure of its symmetrical isomer was determined crystallographically and the corresponding data can be found at the CCDC. M.A. Alvarez, C. Bois, M.E. García, M.T. Rueda, M. A. Ruiz, CSD Communication, 2018, CCDC 1867401.

[18] M.A. Alvarez, M. Casado-Ruano, M.E. García, D. García-Vivó, M.A. Ruiz, Structural and chemical effects of the P^{t}Bu$_2$ bridge at unsaturated dimolybdenum complexes having hydride and hydrocarbyl ligands, Inorg, Chem 56 (2017) 11336, https://doi.org/10.1021/acs.inorgchem.7b01773, and references therein.

[19] C. de la Cruz, N. Sheppard, A structure-based analysis of the vibrational spectra of nitrosyl ligands in transition-metal coordination complexes and clusters, Spectrochim. Acta Part A 78 (2011) 7, https://doi.org/10.1016/j.saaa.2010.08.001.
[20] M.A. Alvarez, M.E. García, D. García-Vivó, A.M. Guerra, M.A. Ruiz, Nitrosyl Derivatives of the Halide-Bridged Complexes $[M_2Cp_2(\mu\text{-}X)(\mu\text{-}P^tBu_2)(CO)_2]$ (M = Mo, W; X = Cl, I), J. Organomet. Chem. 1012 (2024) 123147, https://doi.org/10.1016/j.jorganchem.2024.123147.
[21] a) R. Melenkivitz, G.L. Hillhouse, Synthesis, structure, and reactions of a nitroxyl complex of iridium(III), *cis,trans*-$IrHCl_2(NH{=}O)(PPh_3)_2$, Chem. Commun. (2002) 660, https://doi.org/10.1039/B111645B;
b) D. Sellmann, T. Gottschalk-Gaudig, D. Haubinger, F.W. Heinemann, B.A. Hess, [Ru(HNO)('pybuS4')], the First HNO complex resulting from hydride addition to a NO Complex ('pybuS4'2− = 2,6-Bis(2-mercapto-3,5-di-tert-butylphenylthio) dimethylpyridine(2−), Chem. Eur. J. (2001) 2099, https://doi.org/10.1002/1521-3765(20010518)7:10<2099::AID−CHEM2099>3.0.CO;2-A;
c) R.D. Wilson, J.A. Ibers, Coordinated nitrosyl hydride: structural and spectroscopic study of dichlorocarbonyl(nitrosyl hydride)bis(triphenylphosphine) osmium(II), Inorg. Chem. 18 (1979) 336, https://doi.org/10.1021/ic50192a026.
[22] P. Pyykkö, M. Atsumi, Molecular double-bond covalent radii for elements Li-E112, Chem. Eur. J. 15 (2009) 12770, https://doi.org/10.1002/chem.200901472.
[23] J.E. Huheey, E.A. Keiter, R.L. Keiter, Inorganic Chemistry: Principles of Structure and Reactivity, 4th ed., HarperCollins College Publishers, New York, USA, 1993, p. 301.
[24] K.M. Miranda, The chemistry of nitroxyl (HNO) and implications in biology, Coord. Chem. Rev. 249 (2005) 433, https://doi.org/10.1016/j.ccr.2004.08.010.
[25] M.A. Alvarez, M.E. García, D. García-Vivó, M.A. Ruiz, A. Toyos, E.-H. Bond, Activation and Insertion Processes in the Reactions of the Unsaturated Hydride $[W_2Cp_2(\mu\text{-}H)(\mu\text{-}PPh_2)(NO)_2]$, Inorg. Chem. 57 (2018) 2228, https://doi.org/10.1021/acs.inorgchem.7b03111.
[26] P. Schollhammer, E. Guénin, F.Y. Pétillon, J. Talarmin, η^1-η^2 rearrangement and protonation of phenyldiazo bridging ligands attached to the dimolybdenum System $\{Mo_2Cp_2(\mu\text{-}SMe)_3\}$, Organometallics 17 (1998) 1922, https://doi.org/10.1021/om971114v.
[27] M.D. Fryzuk, S.A. Johnson, The continuing story of dinitrogen activation, Coord. Chem. Rev. 200-202 (2000) 379, https://doi.org/10.1016/S0010-9545(00)00264-2.
[28] Y. Tanabe, Y. Nishibayashi, Transition-Metal Dinitrogen Complexes: Preparation and Reactivity, Y. Nishibayashi (Ed.), Wiley-VCH, Weinheim, Germany, 2019, chapter 1.
[29] D. Singh, W.R. Buratto, J.F. Torres, L.J. Murray, Activation of Dinitrogen by Polynuclear metal complexes, Chem. Rev. 120 (2020) 5517, https://doi.org/10.1021/acs.chemrev.0c00042.
[30] a) For some examples, see for instance Y. Ishida, S. Hasegawa, H. Kawaguchi, Dinitrogen functionalization with carbon dioxide and carbon disulfide giving symmetric and Unsymmetric Hydrazido complexes, Angew. Chem. Int. Ed. 62 (2023) e202304700, https://doi.org/10.1002/anie.202304700;
b) K. Ding, A.W. Pierpont, W.W. Brennessel, G. Lukat-Rodgers, K.R. Rodgers, T. R. Cundari, E. Bill, P.L. Holland, Cobalt-Dinitrogen Complexes with Weakened N-N Bonds, J. Am. Chem. Soc. 131 (2009) 9471, https://doi.org/10.1021/ja808783u, and references therein.
[31] W.L.F. Armarego, C. Chai, Purification of Laboratory Chemicals, 7th ed., Butterworth-Heinemann, Oxford, U. K., 2012.
[32] *CrysAlis Pro*, Oxford Diffraction Limited, Ltd., Oxford, UK, 2024.
[33] L.J. Farrugia, WinGX suite for small-molecule single-crystal crystallography, J. Appl. Crystallogr. 32 (1999) 837, https://doi.org/10.1107/S0021889899006020.
[34] L. Palatinus, G. Chapuis, SUPERFLIP– a computer program for the solution of crystal structures by charge flipping in arbitrary dimensions, J. Appl. Crystallogr. 40 (2007) 786, https://doi.org/10.1107/S0021889807029238.
[35] a)G.M. Sheldrick, SHELXL2018; University of Gottingen, Germany, 2018. b) G. M. Sheldrick, Crystal structure refinement with SHELXL, Acta Crystallogr. Sect. 71 (2015) 3, https://doi.org/10.1107/S2053229614024218. C;
c) G.M. Sheldrick, A short history of SHELX, Acta Crystallogr. Sect. 64 (2008) 112, https://doi.org/10.1107/S0108767307043930. A.
[36] APEX3 v2019.11-0, Bruker AXS Inc., Madison (WI), USA, 2019.
[37] SAINT v8.40B, Bruker AXS Inc., Madison (WI), USA, 2018.
[38] L. Krause, R. Herbst-Irmer, G.M. Sheldrick, D. Stalke, Comparison of silver and molybdenum microfocus X-ray sources for single-crystal structure determination, J. Appl. Cryst. 48 (2015) 3, https://doi.org/10.1107/S1600576714022985.
[39] M.J. Frisch, G.W. Trucks, H.B. Schlegel, G.E. Scuseria, M.A. Robb, J.R. Cheeseman, G. Scalmani, V. Barone, G.A. Petersson, H. Nakatsuji, X. Li, M. Caricato, A.V. Marenich, J. Bloino, B.G. Janesko, R. Gomperts, B. Mennucci, H.P. Hratchian, J.V. Ortiz, A.F. Izmaylov, J.L. Sonnenberg, D. Williams-Young, F. Ding, F. Lipparini, F. Egidi, J. Goings, B. Peng, A. Petrone, T. Henderson, D. Ranasinghe, V.G. Zakrzewski, J. Gao, N. Rega, G. Zheng, W. Liang, M. Hada, M. Ehara, K. Toyota, R. Fukuda, J. Hasegawa, M. Ishida, T. Nakajima, Y. Honda, O. Kitao, H. Nakai, T. Vreven, K. Throssell, J.A. Montgomery, Jr., J.E. Peralta, F. Ogliaro, M.J. Bearpark, J.J. Heyd, E.N. Brothers, K.N. Kudin, V.N. Staroverov, T.A. Keith, R. Kobayashi, J. Normand, K. Raghavachari, A.P. Rendell, J.C. Burant, S.S. Iyengar, J. Tomasi, M. Cossi, J.M. Millam, M. Klene, C. Adamo, R. Cammi, J.W. Ochterski, R.L. Martin, K. Morokuma, O. Farkas, J.B. Foresman, D.J. Fox, Gaussian 16, Revision A.03, Gaussian, Inc., Wallingford CT, USA, 2016.
[40] Y. Zhao, D.G. Truhlar, A new local density functional for main-group thermochemistry, transition metal bonding, thermochemical kinetics, and noncovalent interactions, J. Chem. Phys. 125 (2006) 194101, https://doi.org/10.1063/1.2370993.
[41] S. Grimme, J. Antony, S. Ehrlich, H. Krieg, A consistent and accurate ab initio parameterization of density functional dispersion correction (DFT-D) for the 94 elements H-Pu, J. Chem. Phys. 132 (2010) 154104, https://doi.org/10.1063/1.3382344.
[42] D. Andrae, U. Haeussermann, M. Dolg, H. Stoll, H. Preuss, Energy-adjusted ab initio pseudopotentials for the 2nd and 3rd row transition-elements, Theor. Chem. Acc. 77 (1990) 123, https://doi.org/10.1007/BF01114537.
[43] a) P.C. Hariharan, J.A. Pople, Influence of polarization functions on MO hydrogenation energies, Theor. Chim. Acta 28 (1973) 213, https://doi.org/10.1007/BF00533485;
b) G.A. Petersson, M.A. Al-Laham, A complete basis set model chemistry. II. Open-shell systems and the total energies of the first-row atoms, J. Chem. Phys. 94 (1991) 6081, https://doi.org/10.1063/1.460447;
c) G.A. Petersson, A. Bennett, T.G. Tensfeldt, M.A. Al-Laham, W.A. Shirley, J. A. Mantzaris, A complete basis set model chemistry. I. The total energies of closed-shell atoms and hydrides of the first-row elements, J. Chem. Phys. 89 (1988) 2193, https://doi.org/10.1063/1.455064.